High Dynamic Range Imaging Algorithms

Major Project Report

Submitted in partial fulfillment of the requirements

for the degree of

Master of Technology

in

Electronics & Communication Engineering

(Communication Engineering)

By

Harsh Mukeshbhai Shukla

(13MECC16)

Electronics & Communication Engineering Branch

Electrical Engineering Department

Institute of Technology

Nirma University

Ahmedabad-382481

May 2015

High Dynamic Range Imaging Algorithms

Major Project Report

Submitted in partial fulfillment of the requirements

for the degree of

Master of Technology

in

Electronics & Communication Engineering

(Communication Engineering)

By

Harsh Mukeshbhai Shukla

(13MECC16)

Under the guidance of

Dr. Tanish Zaveri

Associate Professor (EC Dept.),

Institute of Technology,

Nirma University, Ahmedabad.

Electronics & Communication Engineering Branch

Electrical Engineering Department

Institute of Technology

Nirma University

Ahmedabad-382481

May 2015

Declaration

This is to certify that

1. The thesis comprises my original work towards the degree of Master of Technology in Communication Engineering at Nirma University and has not been submitted elsewhere for a degree.

2. Due acknowledgment has been made in the text to all other material used.

- Harsh Mukeshbhai Shukla

(13MECC16)

Certificate

This is to certify that the Major Project entitled **"High Dynamic Range Imaging Algorithms"** submitted by **Harsh Mukeshbhai Shukla (13MECC16)**, towards the partial fulfillment of the requirements for the degree of Master of Technology in Communication Engineering, Nirma University, Ahmedabad is the record of work carried out by him under our supervision and guidance. In our opinion, the submitted work has reached a level required for being accepted for examination.The results embodied in this major project, to the best of our knowledge,haven't been submitted to any other university or institution for award of any degree or diploma.

Date: Place: Ahmedabad

Internal Guide

Dr. Tanish Zaveri
(Associate Professor, EC)

Program Co-ordinator

Dr. D. K. Kothari
(Professor, EC)

HOD

Dr. P. N. Tekwani
(Professor, EE)

Director

Dr. K. Kotecha
(Director, IT-NU)

Acknowledgements

The efforts of my MTech thesis would not have been possible without the kind help of many people. I would like to thank all of them from the very bottom of my heart.

I would like to express my great appreciation to **Dr. Tanish Zaveri**, my supervisor, for his continuous encouragement, support and guidance over the last one year. His continuous suggestions were the key factor in completion of this work.

I would like to express my gratitude and sincere thanks to **Dr. K. Kotecha**, Director, IT-NU, **Dr. P. N. Tekwani**, Head of Electrical Engineering Department and **Dr. D.K. Kothari**, Coordinator of M.Tech Communication Engineering program for allowing me to undertake this thesis work.

I wish to thank my friends for their delightful company which kept me in good humor throughout the last one year.

Last but not the least, I would like to express my special thanks to my family for their continuous understanding and support.

-Harsh Mukeshbhai Shukla

13MECC16

Abstract

Real world around us may contain high dynamic range (HDR) scenes but general purpose imaging devices available in the market have low dynamic range (LDR) imaging capability. Dynamic range of any image refers to the ratio of highest possible pixel value to the lowest possible pixel value. This thesis aims to study HDR imaging pipeline which builds a tone mapped HDR image using its multiple differently exposed LDR images. The pipeline consists of two basic algorithms: dynamic range expansion using differently exposed images and dynamic range compression. Thesis discusses their theories, mathematical models and implementation flows. Moreover, thesis introduces our proposed algorithm which helps in selecting appropriate tone mapping operator (TMO) from a TMO dictionary for any particular scene to be captured. The proposed algorithm uses tone mapped image quality index (TMQI) algorithm to evaluate the performance of each tone mapping operator maintained in our TMO dictionary. The importance of our proposed algorithm has also been outlined by comparing performance of each TMO of dictionary and then discussing the process of selecting the final output. The evaluation capability of TMQI algorithm has been demonstrated by surveying eight tone mapping operators performances over eighteen datasets.

Contents

List of Figures

List of Tables

Abbreviation

CCD ..... Charge Coupled Device
CIE ..... International Commission on Illumination
CMOS ..... Complementary Metal Oxide Semiconductor
CRF ..... Camera Response Function
DR ..... Dynamic Range
HDR ..... High Dynamic Range
HDRI ..... High Dynamic Range Imaging
HVSS ..... Human Visual Subspace
IPM ..... Image Processing Module
IQA ..... Image Quality Assessment
ITU ..... International Telecommunications Union
LDR ..... Low Dynamic Range
LED ..... Light Emitting Diode
MB ..... Mega Bytes
NSS ..... Statistical Naturelness
PDF ..... Probability Density Function
RGB ..... Red Green Blue
RGBE ..... RGB Encoding
SSIM ..... Structural Similarity
SVD ..... Singular Value Decomposition
TMO ..... Tone Mapping Operator
TMQI ..... Tone Mapped Image Quality Index

Chapter 1

Introduction

The human eye can visualize things which reflect or emit light in the range of 360nm to 830nm wavelength. This range is referred to as the visible range of the electromagnetic spectrum. Mainly, it can be divided into six different bands: violet, blue, green, yellow, orange and red. In the era of digitization, we use either CCD or CMOS sensor to capture these color bands in analog form and then we convert them into small digital values called pixel. Such transformation from light intensities to their corresponding pixel values and their applications demand research in the following fields:

- Image Acquisition
- Image Processing
- Image Analysis
- Image Understanding

Image acquisition and image processing work for enhancing experience of image capturing and application based further modification. On the other side, image analysis and image understanding work for improving the overall imaging experience and extracting useful information out of the captured image.

As human eye can differentiate more between color shades than gray shades, colors

are critically more important parameter to enhance image processing performance. Also, colors help us to recognize different objects from a scene and extract the target object out of it. Hence, we use color image processing instead of image processing.
Many researchers have developed different kind of algorithms for color image processing in the areas of: image enhancement, image segmentation, image sharpening, image smoothing, noise reduction, image compression, dynamic range expansion, dynamic range compression (tone mapping) etc. We have studied and analyzed two of them here in this thesis. We have also implemented them on a matlab based platform and assessed their performances with three assessment methods.

1.1 Motivation

In the new era of smart systems, scientists and researchers are trying to put intelligence in every system. Putting intelligence in any system demands to educate it to be independent where independency means sensing inputs and taking right decisions automatically. Image processing can play a major role in this task where we use different kind of algorithms to acquire, process and understand the scene and then taking decisions based on them.
As the beautiful world around us contain very high dynamic range scenes and available general purpose imaging devices have low dynamic range imaging capability, the research scopes are very huge in the field of HDR imaging.Also, the field of digital photography is demanding more realistic images i.e. an extension of dynamic range from LDR to HDR. The high dynamic range imaging can be very helpful in solving these problems.

1.2 Problem Statement

Although the problem of capturing high dynamic range scenes can be solved by high dynamic range imaging devices (hardware based solution), it is quite expensive to

adapt it in normal use. However, we can also solve this problem with help of HDR imaging algorithms (software based solution) which take differently exposed images of the same scene using general purpose low dynamic range imaging device and then fuse them together to obtain a high dynamic range image.
Main motives of this thesis are studying and implementing HDR imaging algorithms and solving the problem of tone mapping operator selection with respect to present scene to be captured through our proposed algorithm.

1.3 Applications

Applications in which colors and their intensities are needed to be met with an excellence, we use HDR imaging. Some examples of such applications are as given below:

- **Physically Based Rendering:** Normally, we would be more interested in recording, storing and displaying scenes which are in the range of human visual system but image based rendering tries to cover more than what human visual system can actually perceive. So that, HDR imaging can help us to come up with a software based solution for it.

- **Remote Sensing:** Images taken from satellite may go out of low dynamic range. Therefore, if we use LDR capturing methods for remote sensing application, we may lose some important data. So, we use HDR imaging algorithm to expand the dynamic range of captured scene.

- **Digital Photography & Image Editing:** In the era of digitization, digital imaging devices have got a huge response from professional photographers as well as consumers. Moreover, camera makers are putting more efforts to capture even more realistic images which need an extension of dynamic range. This can be achieved using HDR imaging algorithm.

- **Digital Cinema:** The most important application of HDR imaging is digital cinema. Digital cinema also adapts the updates in HDR imaging continuously to make the best out of it. Recording and displaying scenes in high dynamic range changes the whole experience of audience. In this process, color intensity levels, resolution and information size also matter a lot for digital cinema. HDR imaging also help us to maintain balance between these three things.

- **Virtual Reality:** Some web applications demand experience of virtual reality. As transmission of images may result into erroneous data due to lossy encoding, maintaining a proper exposure of transmitted image is very tough. Hence, we need proper standards for storing and transmitting our images. HDR imaging algorithm is basis for such standards.

- **Computer Games:** The animations and graphics used in high end games need image-based rendering and perceptually based dynamic range compression. These things add more realistic experience. Hence, we use HDR imaging algorithm in such application's image processing pipeline.

1.4 Thesis Organization

The overall work has been divided into five chapters:
The first chapter introduces HDR imaging algorithm as a part of color image processing. It also provides motivation to work on HDR imaging by explaining its importance and possible range of applications. Lastly, it discusses the flow thesis.
The second chapter covers important definitions and concepts used in thesis such as working of human eye and digital camera, color spaces, etc. Moreover, it also discusses two important algorithms used in HDR imaging where it covers their theory, mathematical modeling and implementation flow. In short, this chapter provides a complete literature survey for HDR imaging.
The third chapter introduces our proposed algorithm and discusses its importance in

HDR imaging pipeline. It also explains working of our proposed algorithm.

The fourth chapter shows results of basic HDR imaging pipeline and then discusses the importance of our proposed algorithm by showing its contribution in getting best possible output for HDR imaging. Moreover, it shows the objective as well as subjective survey of tone mapped HDR output images for all datasets. This survey illustrates the capability of TMQI algorithm to evaluate the performance of any tone mapping operator.

The fifth chapter enlists the importance of HDR imaging algorithm and its significance in real world applications. It also enlists the problem overcame in HDR imaging algorithm by our proposed algorithm. Lastly, it discusses future scopes for further research in this field.

Chapter 2

Literature Survey

2.1 Human Eye

The field of digital image processing has founded on mathematical and probabilistic formulations. Human intuition and analyses play a major role in comparing different techniques of image processing. Hence, it is very important to gain basic understanding of human visual system as it is the very first step in our journey throughout our research work in this thesis. Firstly, we will understand the structure of human eye using a rough schematic. Then, we will try to understand the working of human eye mathematically. Such mathematical model of human eye can help us in comparing human visual system with digital camera.

2.1.1 Structure

The human eye is one of the most sensitive and valuable part of our body. We can easily understand eye's light gathering capability by considering its following parts: cornea, iris, pupil, lens, retina and blind spot. These parts have been shown in figure 2.1. The front part of human eye is covered by transparent spherical membrane called the cornea which focuses the incident light into the eye. Behind the cornea, there will be a dark colored muscular diaphragm which will have a small circular opening in its

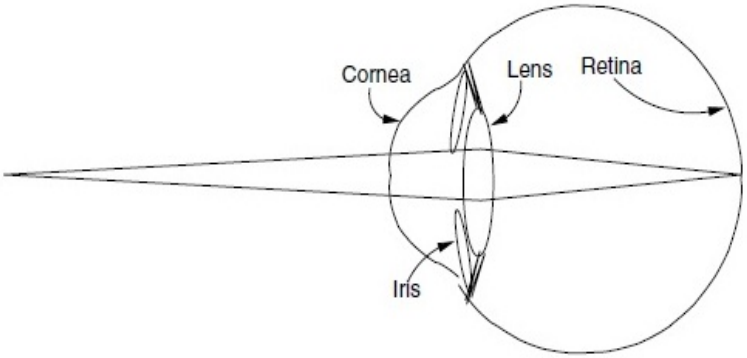

Figure 2.1: Human Eye

middle. That small circular opening is known as pupil. Generally, pupil appears to be black as no light can be reflected back from it. According to the lightening condition of surroundings, pupil adjusts its size to decide amount of light which should enter through it. Then, there would be a eye lens which is made up of a transparent jelly type proteinaceous material. It is hard at the middle but gradually becomes soft as we move from centre to outer edges. Ciliary muscles help to set curvature and focal length of lens. At last, the light fall onto the retina which work as a sensor for eye. It consists of two types of light sensitive receptors: rods and cones.

Rods are very sensitive to light but they are not much involved in color vision. There are three kind of cones: S cones (sensitive to small wavelengths), M cones (sensitive to medium wavelengths) and L cones (sensitive to large wavelengths). Cones are mainly responsible for color vision. Rods will be active in scotopic vision, cones will be active in photopic vision whereas both will be active in mesopic vision (intermediate vision). Upto this point, light gathering work has been done. Then after, an optic nerve connects eye with human brain. Human brain do process of light perception i.e. brain interpret light into information. Point at which an optic nerve enters into eye is called the blind spot as it is insensitive to light. Like this, whole process of gathering the light by eye and then interpreting it with help of brain completes.

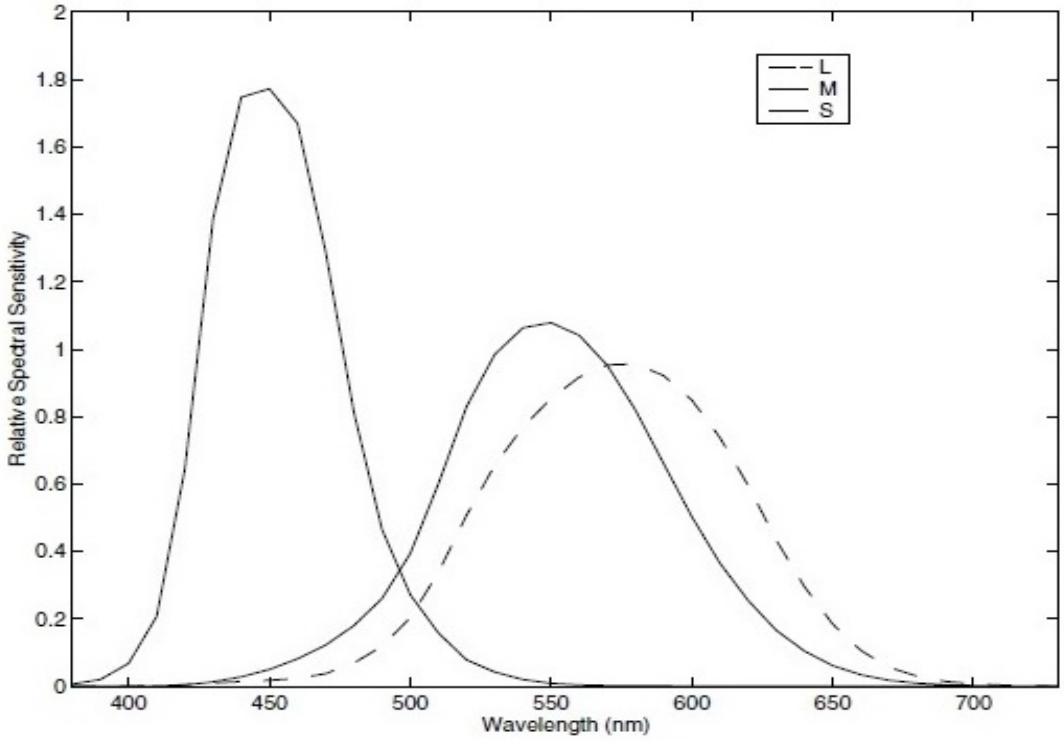

Figure 2.2: Sensitivities of LMS cones

2.1.2 Working

Under certain assumptions, we can model responses of three cones by a linear system using their spectral sensitivities by equation 2.1. Human eye can visualize between wavelength range of 360 nm and 830 nm only. The estimation of effective sensitivities of the LMS cones can be shown as figure 2.2. The total range of wavelength covered by these three cones is known as human visual subspace (HVSS).

$$C_i = \int_{\lambda_{min}}^{\lambda_{max}} \{S_i(\lambda) f(\lambda)\} d\lambda \; ; \; i = 1, 2, 3 \tag{2.1}$$

Where, λ denotes the wavelength, $f(\lambda)$ is the spectral distribution of light incident on retina, $S_i(\lambda)$ represents the sensitivity of ith type of cones, and λ_{min} to λ_{max} is the range of wavelength out of which the value of sensitivity will be zero.

2.2 Digital Camera

Digital camera is a fantastic piece of art which has been inspired by the human eye. It help us to capture important or informative moments and then convert it into a digital form for display or further process. The number of consumers, professional photographers and applications of it are increasing drastically day by day.
Digital camera's hardware architecture and image processing pipeline supported by its firmware decides its real capabilities and performance level. Mainly, its work is to convert light into electrical charges which can be stored easily.

2.2.1 Working

Small light particles called photons start travelling from source. When they strike with any object, some of them will be reflected back which enter into our imaging device. Such amount of waves with particular wavelength decides the color and its intensity to our imaging device.
When these photons enter into a digital camera, first of all they pass through a series of lenses which allow photographer to decide what he wants to capture and on what he wants to focus. Basically, lenses help us to gather proper light and direct it towards aperture.
Aperture decides the amount of light that will go toward a mirror or image sensor. Until photographer presses capturing button, the light will be bounced off by a mirror and after passing through a prism, it reaches view finder.
Whenever photographer presses capturing button, the mirror will be lifted upward and light will move towards the sensor. Generally, sensor may be either charged coupled device(CCD) or complementary metal oxide semiconductor(CMOS). Sensors are heart of a digital camera.
They are made up of tightly structured grid of very small light sensors. When photons collide with sensor, they will be absorbed and then converted to electronic particles

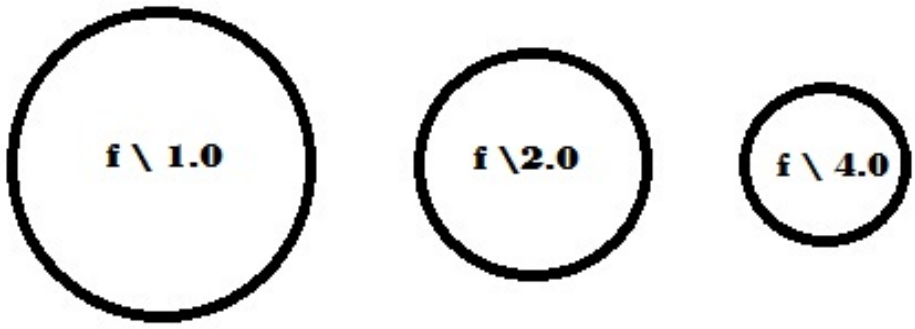

Figure 2.3: Aperture value and its corresponding size

called electrons i.e. an electrical charge. As brightness of scene increases, intensity of electrical charge increases. Then, a circuit board associated with sensor converts these intensities into digits (1s and 0s). Like this, light will be converted into digits.

2.2.2 Digital Camera Vs. Human Eye

In human visual system (HVS), eye captures light and brain interprets it into meaningful information intelligently. On the other side, a digital camera simply captures light and stores it in a particular image format. So, the main advantage of human visual system is its intelligent perceptual capability. Moreover, we can also compare them based on their angle of view, resolution, dynamic range, etc. As our thesis targets to improve the dynamic range of a digital camera, we will compare them based on their dynamic ranges only.

The dynamic range (DR) can be given for either a scene or a sensor. For a scene, it is the range from highest available intensity to the lowest available intensity in it. For a sensor, it is ratio of the highest light intensity to the lowest light intensity that it can sense in a single and/or multiple scenes. Sometimes, it is also called as contrast ratio. Human eye can perceive light over range of 5 orders of magnitude simultaneously. Moreover, the adaptive capabilities of pupil expand this range up to 10 orders

of magnitude, which helps us to perceive scenes ranging from as low as starlight to as high as sunlight. In comparison with human eye, modern digital cameras can capture only over a small dynamic range of about three orders of magnitude in a single exposure which will result in information loss from very bright and/or very dark areas. Such areas are known as saturated areas. According to its range, we define dynamic range either by low dynamic range (LDR) or high dynamic range (HDR). General purpose display devices and printers work on LDR whereas HDR is being used in medical and astronomical applications. In the following section, we will see how to capture an HDR scene using LDR digital camera and how to transform that HDR image into a meaningful LDR image so that we can display it on general purpose LDR display devices.

2.2.3 Camera Response Function

The radiance values are mapped to their corresponding pixel values after passing through image sensor and image processing module (IPM). This whole process can be represented as a function which is known as camera response function (CRF). It can be expressed as,

$$Z = f(X) \tag{2.2}$$

Here, X is radiance value, Z is its corresponding pixel value and f represents the CRF. CRF for our input images of dataset 1 used in chapter 4 is shown in Figure 2.4. After obtaining this curve, we can actually estimate the original radiance value X of any pixel from its pixel value Z. Therefore, this curve can be very helpful in obtaining a high dynamic range image from its various low dynamic range images.

2.2.4 Exposure Settings

Exposure settings play a major role in capturing colors the way actually they are. They decide intensity value of each pixel in captured photograph. Exposure settings consist of three different settings:

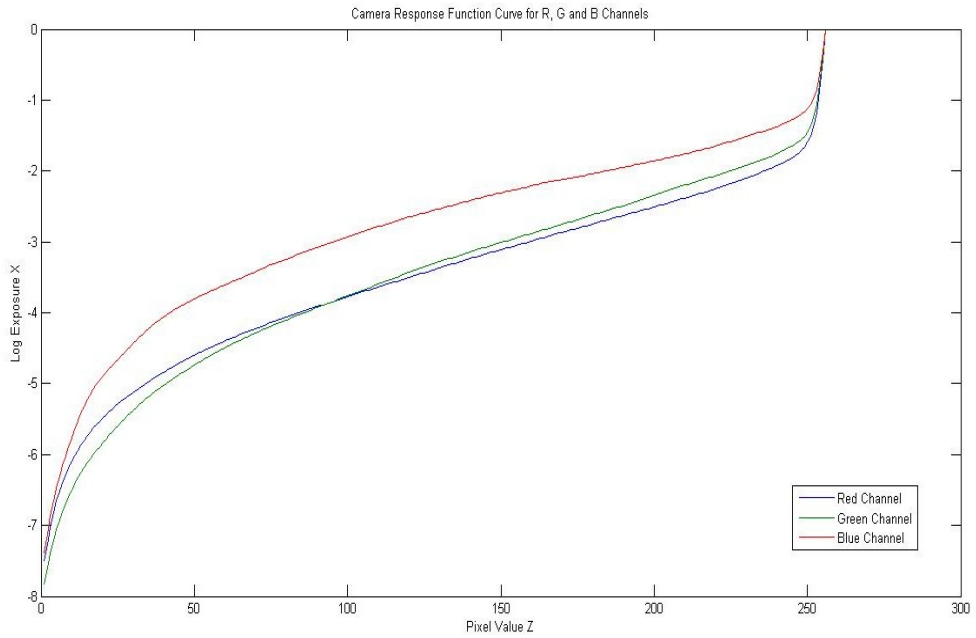

Figure 2.4: Camera Response Function for R, G and B Channels

- Aperture value
- Shutter speed
- ISO speed

As these three things decide exposure settings, we can achieve the same exposure settings with help of several combination. These three things influence the scene visualization experience by our imaging device. Therefore, we need to choose which trade-offs are suitable for our application.

Aperture value: An aperture value decides the amount of light which will be allowed to enter the camera. Generally, we represent it in terms of f-stop values. As value of f-stop increases, the area from which light can come in decreases. It can be easily seen in figure 2.3. When f-stop value doubles, the light gathering area decreases by four times.

Shutter speed: Shutter speed decides the amount of time up to which light will be allowed to enter the camera. The relationship between shutter speed and exposure setting is as simple as 1:1 correlation. Like, if we half the value of shutter speed, the

amount of light entering camera also halves. Sometime we also refer it as exposure time as both are based on same concept.

ISO speed: ISO speed is a scale on which we used to measure sensitivity of any sensor. It determines that how tiny changes in quantity of light affects the pixel values. Same as shutter speed, it also encompasses relationship of 1:1 correlation with exposure setting. As sensitivity increases, sensor will sense even very small changes in light quantity and that will result in image noise. This effect forces us to keep its value in certain range.

2.3 Color Spaces

The concept of color spaces can be understood by two ways. Firstly, every color space has different set of formulas which define relationship between a color vector or triplet and the standard CIE XYZ color space. Generally, such relationships can be depicted using a 3 x 3 color transformation matrix.

If the space is nonlinear then there would be additional set of formulas, too. Secondly, it is a two-dimensional boundary on the volume defined by its vector which is usually determined by the maximum value and minimum value out of each primary, the color gamut.There are many types of color spaces available where each of them is used in different kind of tasks.

Mostly, all capturing and displaying devices have their own primaries or color spaces. Such color spaces are referred to as device-dependent RGB. Now a day, we use output-referred standards for image encoding which means that they use a color space which is compatible with its output device.

This ensures that output device will not be needed to convert an incoming image from one color space to another color space which actually help us to improve the speed of communication and also decreases the unnecessary use of resources.

On the other hand, it will limit the flexibility of using any device at the output end and the output image will not be helpful in any further image processing task any

more. Hence, it is advisable to use transformations of color spaces as and when required in between different devices than using output-referred standards.

There are two ways to convert one tristimulus color space into another tristimulus color space:

First method: If xy chromaticity coordinates have been given for primaries and white point as shown in the table I[4] then we can use this method. Here, white point is the color of point where each primary contributes the same. First of all, white point

Table I: xy chromaticity coordinates for primaries and white point specified by ITU-R Recommendation BT.709[4]

	R	G	B	White
x	0.6400	0.3000	0.1500	0.3127
y	0.3300	0.6000	0.0600	0.3290

and its maximum luminance Y_W will be specified. Then, based on all other values, we will determine z chromaticity coordinate for each primaries. Next, we will find tristimulus values (X_W, Y_W, Z_W) from white points chromaticities and its maximum luminance value.

Based on all these values, we will be able to write three linear equations as shown here:

$$X_W = x_R S_R + x_G S_G + x_B S_B \tag{2.3}$$

$$Y_W = y_R S_R + y_G S_G + y_B S_B \tag{2.4}$$

$$Y_W = y_R S_R + y_G S_G + y_B S_B \tag{2.5}$$

Solutions of these three equations will contain values of S_R ,S_G and S_B.

Substituting all these values get us following conversion matrix to convert color space RGB into XYZ as given below:

$$\begin{bmatrix} X \\ Y \\ Z \end{bmatrix} = \begin{bmatrix} x_R S_R & x_G S_G & x_B S_B \\ y_R S_R & y_G S_G & y_B S_B \\ y_R S_R & y_G S_G & y_B S_B \end{bmatrix} \begin{bmatrix} R \\ G \\ B \end{bmatrix}$$

Similarly, conversion from color space XYZ to RGB can be computed by inverting the above matrix.

Second method: If xy chromaticity coordinates for primaries and white point are unknown then we will be using this method. In this method, we will be directly using standard matrix for converting color spaces RGB to XYZ and vice versa. These standard matrices have been specified by the International Telecommunication Union as ITU-R Recommendation BT.709[4]. These matrices were being created from xy chromaticity coordinates for primaries and white point given in Table 2.1.

$$\begin{bmatrix} X \\ Y \\ Z \end{bmatrix} = \begin{bmatrix} 0.4124 & 0.3576 & 0.1805 \\ 0.2126 & 0.7152 & 0.0722 \\ 0.0193 & 0.1192 & 0.9505 \end{bmatrix} \begin{bmatrix} R \\ G \\ B \end{bmatrix}$$

$$\begin{bmatrix} R \\ G \\ B \end{bmatrix} = \begin{bmatrix} 3.2405 & -1.5371 & -0.4985 \\ -0.9693 & 1.8760 & 0.0416 \\ 0.0556 & -0.2040 & 1.0572 \end{bmatrix} \begin{bmatrix} X \\ Y \\ Z \end{bmatrix}$$

Similarly, standard matrices and non-linear transforms are also available for other RGB standards. As per ITU-R recommendation BT.709 RBG, we can directly calculate luminance of any image using following equation[4]:

$$L = \{(0.2126 \times R) + (0.7152 \times G) + (0.0711 \times B)\} \tag{2.6}$$

Here, R,G and B are the red, green and blue channels of image respectively.

2.4 HDR Imaging Algorithms

Color image processing algorithms provide us different ways to mold our available information in a meaningful way according to our application. They use different characteristics of our image to adjust information of an image in a desired form.

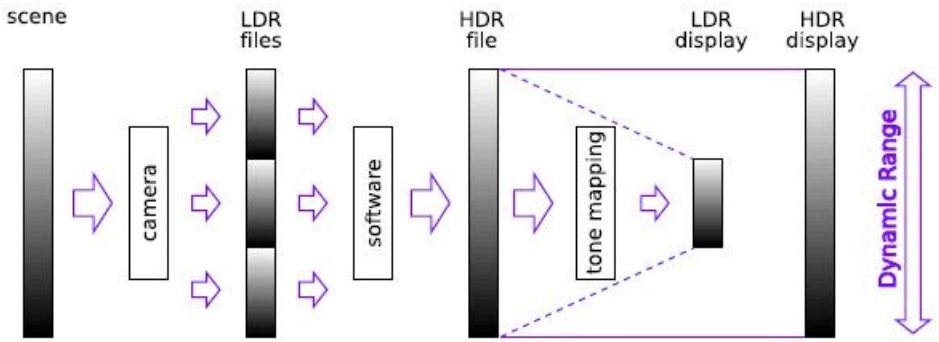

Figure 2.5: The overall process flow of HDR imaging algorithm

For example, the brightness and contrast of any image can be varied using its mean and deviation values. We have studied and implemented two such algorithms here: dynamic range expansion using differently exposed images and dynamic range compression (tone mapping). Here, we have considered the software based solution for achieving dynamic range expansion which is more practical and cost effective with respect to hardware solution. We have used concept of extracting radiance values of any scene from its multiple exposed low dynamic range images to generate a high dynamic range image. On the other side, dynamic range compression can be achieved using various tone mapping operators (TMOs). Therefore, we have studied types of tone mapping operators and the series of steps on which they work. Moreover, we have also studied three assessing methods for tone mapping operators: Modified SSIM, NSS and TMQI. When we cascade these two algorithms, it makes an HDR imaging pipeline. Lastly, we discussed implementation of each algorithm separately and then using them together in cascaded manner. The overall process flow of HDR imaging algorithm has be shown in figure 2.5.

2.4.1 Dynamic Range Expansion using Differently Exposed Images

The dynamic range of general purpose imaging device is very low with respect to dynamic range of the real world scenes. Therefore, capturing any image does not

make sure that we have covered the whole dynamic range available in the scene. Such problem can be solved using four methods [6]:

- Using a hardware which is specially designed to capture HDR scenes directly
- Using software based solution: Obtaining radiance values of scene from differently exposed LDR images of the same scene
- Using software based solution: Widening dynamic range of LDR image using legacy content
- Building a virtual environment with help of physically based renderers which help out to generate HDR content from LDR content

As second method just requires differently exposed images of the same scene to create its high dynamic range image, it is easy to implement. On the other side, remaining three methods are complex as well as costly to implement. These things clearly say that the second method is easiest and practically possible to acquire high dynamic range images. The process of dynamic range expansion of any image from its differently exposed images can be divided into two steps: content generation and content storing. We will also discuss two possible solutions for displaying high dynamic range contents.

In content generation, we extract the radiance values of each pixel from its differently exposed images. Camera response function plays a major role in this step.

In content storing, we use standards which are more robust to organize large numbers such as 32-bit floating point radiance values. Some of available standard formats are also given in table II.

In content displaying, we will discuss two possible solutions for displaying high dynamic range contents: native HDR displays and traditional LDR displays through tone mapping operators.

2.4.1.1 Content Generation

As discussed in section 2.2, light which enters the digital camera passes through a series of lenses and an aperture. Then, it strikes image sensor after passing through a prism. Sensor takes photons as input and gives electrons as output. These charges will be passed through analog to digital conversion and remapping for our convenience. At last, we are left with digital values called pixel values. Such process steps with their respective denotations of light intensity values can be depicted in figure 2.6. Here, j denotes number of photograph and i denote the number of pixel in j^{th} photograph. Moreover, we take certain assumptions for our convenience. Assumptions for these photographs are:

- The scene in photograph does not contain any moving object i.e. static scene
- All photographs are taken with same camera without moving position of it
- Natural lightening in the scene has not changed during capture time of all photographs
- Exposure time for each photograph is different

The exposure value(X_{ij}) can be given by product of the irradiance value(E_i) and its exposure time(Δt_j)[7], so that,

$$X_{ij} = E_i \Delta t_j \quad (in\ Jm^{-2}) \tag{2.7}$$

As shown in figure 2.6, the function involved in transforming exposure value X into pixel value Z is known as camera response function (CRF). It is a nonlinear function and we assume it to be constant for the same digital camera in any condition. Let us define such nonlinearities of characteristic curve of sensor and further processes steps using f. Here, we assume that f is monotonically increasing function so that it can be inversed i.e. f^{-1} can be defined.

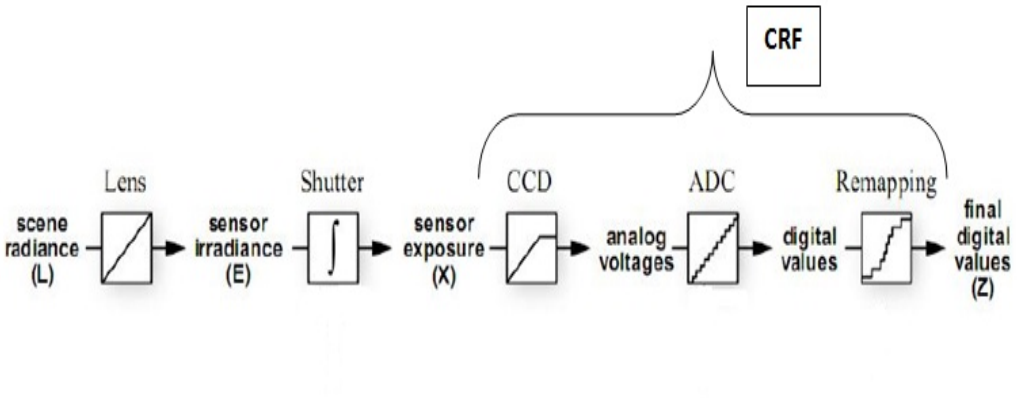

Figure 2.6: Image Acquisition Pipeline[7]

So that, we can write,

$$Z_{ij} = f(X_{ij}) \tag{2.8}$$

Putting value of X_{ij},

$$Z_{ij} = f(E_i \Delta t_j) \tag{2.9}$$

We can write it as,

$$f^{-1}(Z_{ij}) = E_i \Delta t_j \tag{2.10}$$

Taking natural logarithm on both sides, we get,

$$lnf^{-1}(Z_{ij}) = lnE_i + ln\Delta t_j \tag{2.11}$$

To make it simple, let us consider $g = lnf^{-1}$, therefore g will also be a monotonic and smooth function, now we get[7],

$$g(Z_{ij}) = lnE_i + ln\Delta t_j \tag{2.12}$$

In equation (3.6), values of Z_{ij} and Δt_j are known but values ofE_i and function g are unknown. So, we wish to get back the values of E_i and function$g$ with a method of least squared error sense. To know function g, we need to find values that it can

take as output. As function g has finite number of input values ($Z_{ij}\epsilon[Z_{min}, Z_{max}]$) , it will also have finite number of output values. If we recover these all possible ($Z_{max} - Z_{min} + 1$) output values of function g, we get function g. Let, Z_{min} be the minimum value of a pixel, Z_{max} be the maximum value of a pixel, N be the total number of pixels in one photograph and P be the total number of photographs.
We can define a quadratic objective function as[7],

$$O = \sum_{i=1}^{N}\sum_{j=1}^{P}\Big[g(Z_{ij} - ln\ E_i - ln\ \Delta t_j)\Big]^2 + \lambda \sum_{z=Z_{min}+1}^{Z_{max}-1} g^{''}(z)^2 \tag{2.13}$$

In equation (3.7), the first term on right side give surety of satisfying the set of equations defined by equation (3.6) in a least squared sense. Second term contain summation of squared vales of second derivatives of function g, which is called smoothness term. This term ensures that function g is smooth. Generally for discrete values, we take $g^{''}(z) = g(z-1) + 2g(z) + g(z+1)$. We have also used a weighting scalar λ to balance out between smoothness term and data fitting term. Value of λ can be chosen according to the noise available in values of input values Z_{ij}. Furthermore, we solve equation (3.7) using singular value decomposition (SVD) method[7].
After retrieving back $g(z)$ from equation (3.7), if we carefully analyze its curve, we will come to know that it has a sharp slope near values Z_{min} and Z_{max}. This behavior will degrade our smoothness at those points on curve. To eliminate this, we define a weighting function$w(z)$. Weighting function will be defined in such a way that it will maintain smoothness at these points on curve. Malik and debevec have used a simple hat function as shown below[7]:

$$w(z) = z - Z_{max}, z \leq 0.5(Z_{min} + Z_{max}) \tag{2.14}$$

$$w(z) = Z_{max} - z, z = 0.5(Z_{min} + Z_{max}) \tag{2.15}$$

When we use weighting function, our equation (3.7) becomes[7],

$$O = \sum_{i=1}^{N}\sum_{j=1}^{P} w(z)\Big[g(Z_{ij} - ln\ E_i - ln\ \Delta t_j)\Big]^2 + \lambda \sum_{z=Z_{min}+1}^{Z_{max}-1} w(z)g^{''}(z)^2 \tag{2.16}$$

Since the set of linear equations arising from equation (3.7) is very large, we cannot use all of them due to computational complexity.So we choose some of pixels out of whole image for further process. Selection of pixels should be done on following basis:

- They should be evenly distributed over the range of Z_{min} to Z_{max} which also ensures that selected pixels are evenly distributed over spatial plane.
- They should be selected from low intensity variance which decreases the consequence of optical blur due to imaging device.

After recovering function g, we use it to get radiance values from given pixel values and exposure timing for each photograph. Function g can be used for any photograph taken by the same imaging device. From equation (3.6), we can write[7],

$$lnE_i = g(Z_{ij} - ln\Delta t_j) \tag{2.17}$$

We use all available differently exposed pixel values to get radiance value of each pixel. It improves our robustness of achieved radiance values. Weighting function can be used as[7],

$$lnE_i = \frac{\sum_{j=1}^{P} w(Z_{ij})(g(Z_{ij}) - ln\Delta t_j)}{\sum_{j=1}^{P} w(Z_{ij})} \tag{2.18}$$

Such method improves accuracy in recovering radiance values and increases immunity over noise.

2.4.1.2 Content Storing

Once HDR content is being captured, we need to store it for future work or to display it. HDR content contains three single floating point values for each color channels

i.e. red, green and blue[6]. The same scene which takes up 6 MB of space for LDR imaging needs approximately 24 MB for HDR imaging. Therefore, we need a more organized, more efficient and a compact format which can systematize the HDR content effectively. In the beginning, ward introduced a method called RGBE which can help to store HDR radiance values. Then after, many formats and methods have been introduced to do so which are shown in Table II[4]. Also, other important information is given in Table III[4].

Table II: Formats for HDR[4]

Format	Encoding(s)	Compression
HDR	RGBE	run-length
	XYZE	run-length
TIFF	IEEE	RGB none
	LogLub24	none
	LogLuv32	run-length
EXR	Half RGB	Wavelet, ZIP

Table III: Details of HDR Encoding standards[4]

Encoding	**Color Space**	**Bits/pixel**	**Dynamic Range Range**(log_10)	**Relative Error(%)**
Srgb	RGB in [0,1] range	24	1.6 orders	Variable
Rgbe	Positive RGB	32	76 orders	1.0
TIFF	IEEE	RGB none	76 orders	1.0
	LogLub24	none	79 orders	0.000003
	LogLuv32	run-length	4.8 orders	1.1
EXR	Half RGB	Wavelet, ZIP	10.7 orders	0.1

2.4.1.3 Content Displaying

The sole purpose of generating high dynamic range image is to improve visualization quality of any image. The generated content can be visualized using two solutions: native HDR displays and traditional LDR displays through tone mapping operators.

Native HDR display devices have a very high dynamic range i.e. 10,000:1. They do not need tone mapping operators to scale down high dynamic range into low dynamic range. Some of the available devices with their basic details are enlisted in Table IV[6]. Moreover, these devices are also shown in 2.7 [4][6].

Table IV: Native HDR display devices[4]

Device Name	L_{min} **in cd**m^2	L_{max} **in cd**m^2	**Dynamic Range**
HDR Viewer	0.5	5,000	10,000:1
HDR Monitor: Projector-based	0.054	2,700	50,000:1
HDR Monitor: LED-based 37	0.015	3,000	2,00,000:1

As native HDR displays are very costly and also in its developing stage, we prefer traditional LDR displays to visualize HDR content using tone mapping operators more. Detailed information about tone mapping operator is given in section 3.2.

2.4.1.4 Algorithm Implementation

The goal of our algorithm is to take more than one LDR images as input and return a single HDR image in output. The output image should be in .hdr format. For simplicity, we divide our whole algorithm in five blocks. The flow of process in our algorithm is illustrated using a simple block diagram which is shown in figure 2.8.
The importance of each block in our algorithm is described here:

Read LDR Stack: It reads differently exposed LDR images from a target folder and then stores the information of each image into different matrices.

Ward Alignment: As we are not sure that each input image set will be properly aligned (ordered from lightest to darkest image), we need to make it sure to get the best out of our algorithm. Therefore, we consider each image and align them one after another by comparing them with each other.

Read LDR Exposure Timings: Each differently exposed image will have its corresponding exposure timing which can be very helpful in finding the radiance values of each pixel. Generally, we store these exposure timings in a .txt file. This block

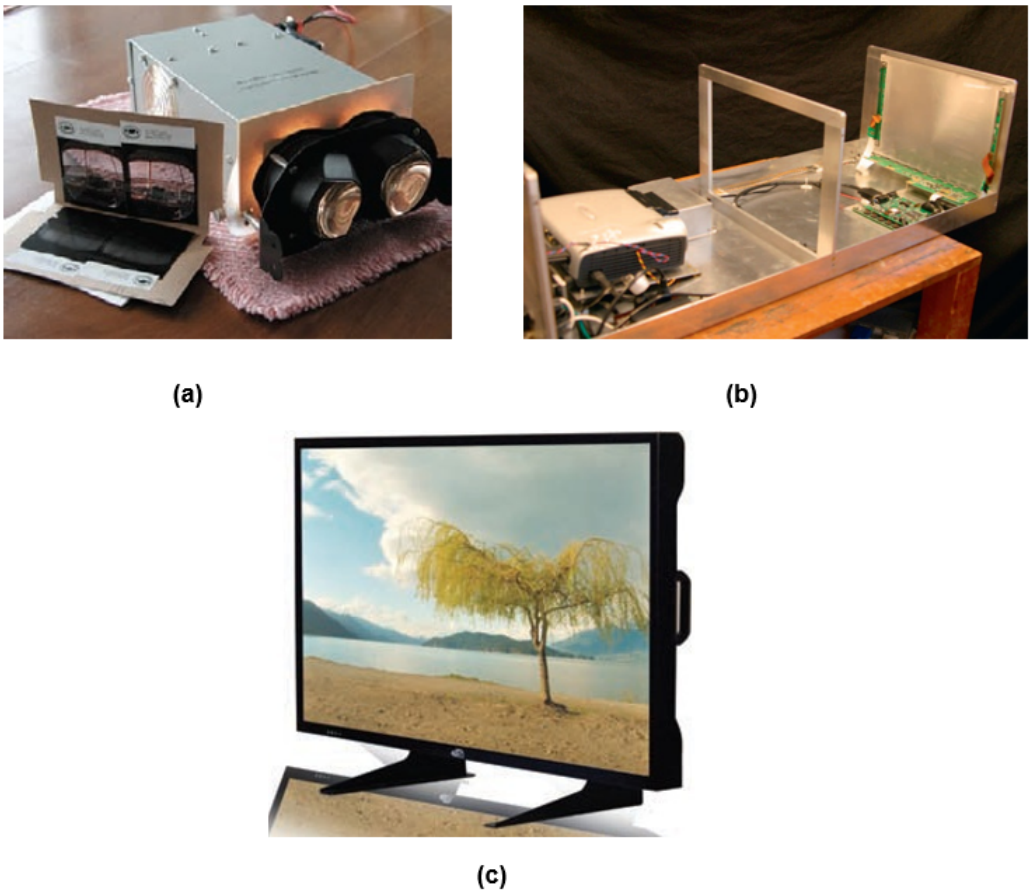

Figure 2.7: (a) HDR Viewer[6] (b) HDR Monitor: Projector-based[4] (c) HDR Monitor: Grand Cinema SOLAR 47 by SIM 2[6]

extracts those values directly from that .txt file and it stores them in vector form.

Build HDR: This block performs the most important role in our algorithm. It takes output of last two blocks and manipulates two things:

- Camera response function (CRF) curve (f)
- Radiance values (E_i)

The matlab function "gsolve.m" given in the reference[7] has been used in this block to compute radiance values from its known pixel values and exposure timings.

Write HDR Image: This block takes the generated radiance values from the last block. Then it applies a RGBE encoding with a run-length compression to it. Lastly,

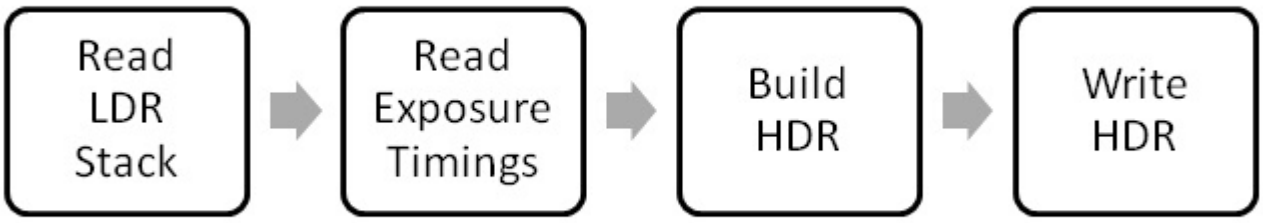

Figure 2.8: Block diagram for dynamic range expansion using differently exposed images of the same scene

it stores the overall floating point data with .hdr format in a well organized manner. The algorithm of this block has been introduced by Greg Ward and it is used from reference[6].

2.4.2 Dynamic Range Compression

As we are not able to display HDR content directly on ordinary LDR screens, we scale down our high dynamic range of real-world scenes onto a low dynamic range that can be displayed by ordinary LDR screens. This process is generally referred to as tone mapping or tone reproduction. The tone mapping, transformation from high dynamic range to low dynamic range, can be obtained by either linear scaling of luminance values or logarithmic scaling of luminance values. A good dynamic range compression allows us to produce an image that is almost perceptually similar to that of the original image. To excel in this solution, we should think of it by keeping human visual system in mind. As human eyes response to the light is purely logarithmic, a logarithmic scaling produces more recognizable low dynamic ranged output image. Although the linear scaling is simplest scaling operation, it removes a significant amount of our information. Logarithmic scaling uses natural log operation

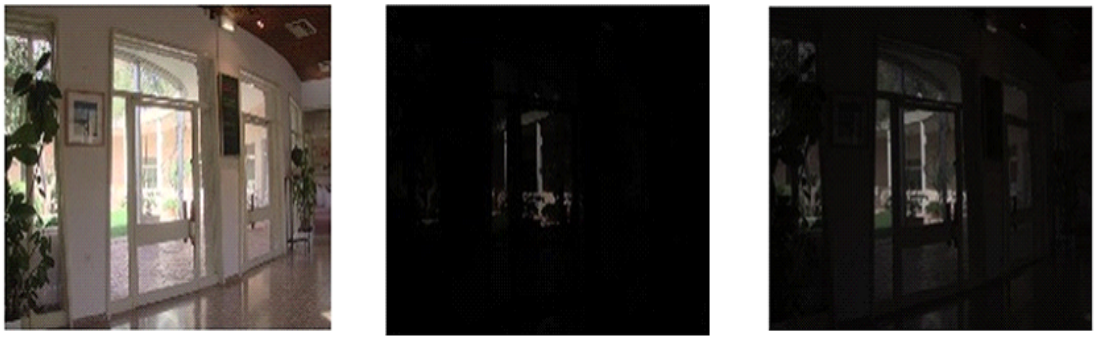

Figure 2.9: Difference of scaling: (a) Original LDR Image (b) Linearly scaled image (c) Logarithmically scaled image

on all HDR radiance values which shifts almost all HDR radiance values into LDR which make it compatible for ordinary display devices. This difference can be easily observed from figure 2.9. Such approach helps us to restore much of the detail from HDR radiance values in LDR values but it also desaturates both color and contrast. Many of the tone mapping algorithms work with logarithmic domain and each of them suffers from different logarithmic compression deficiencies.

2.4.2.1 Types of Tone Mapping Operator

Furthermore, tone mapping can be subdivided into two categories:

1. Global tone mapping operator
2. Local tone mapping operator

Global tone mapping operator: In global tone mapping, we use a single spatially invariant mapping function for all the pixels of an image. Thus, it is very simple to use. As high contrast appearance is very difficult to achieve with them, they have received somewhat less attention of researchers. On the other side, they are much more efficient and they do not have halo-artifacts like many local operators do.

Local tone mapping operator: In local tone mapping, we apply adaptive mapping

functions to local pixel statistics and the local pixel content of an image. Thus, it is difficult to us with respect to global tone mapping operators. In it, we need to continuously set a number of parameters empirically which make it computationally very intensive and also harder to get it on the way we wanted it to be.

2.4.2.2 Assessment Methods for TMO

As many TMOs are available, it is difficult to choose best possible TMO for our application of use. Therefore, we use image quality assessment (IQA) methods to compare reference HDR image and its tone mapped LDR image by several TMOs. IQA methods can be classified into two types: objective and subjective.

Subjective IQA method: It manipulates the ratings given by human observers to characteristics of an image such as image contrast, image brightness and colors. As such methods are time consuming, expensive and they have their own limitations, we cannot consider them as a golden standard.

Objective IQA methods: They directly deal with the characteristics of an image. Also, it does not demand any human observation which make it easier and less time consuming with respect to objective IQA method. We are going to discuss three subjective methods here:

1. Modified structural fidelity (Modified SSIM)
2. Statistical naturalness (NSS)
3. Tone mapped image quality index (TMQI)

Modified SSIM: Multi-scale structural fidelity is nothing but a modified version of SSIM. It provides a practical way to measure structural fidelity between two images. It divides both HDR and its tone mapped LDR image in local patches and then it compares each LDR local patch with its corresponding HDR local patch. First, it calculates the signal strength of LDR local patch and its corresponding HDR local patch. Then, it checks whether these signal strengths are lying in visibility threshold

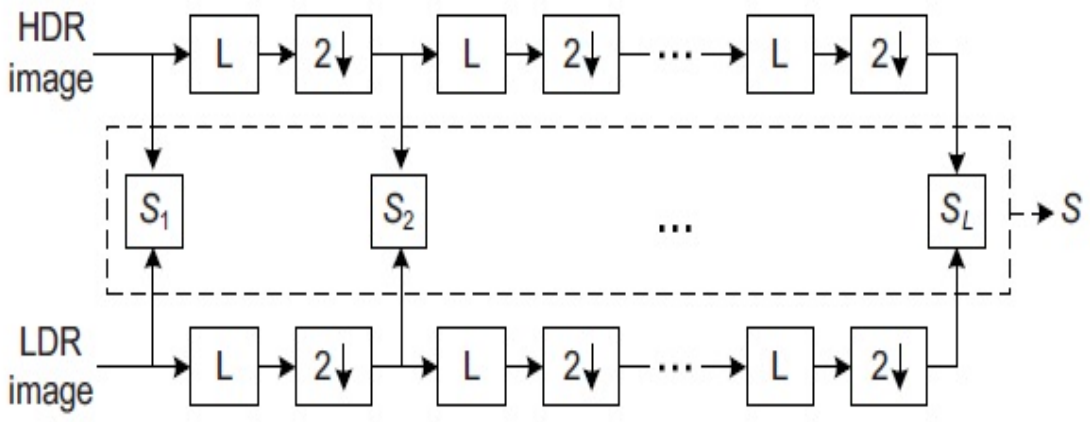

Figure 2.10: The overall frame work of multi scale SSIM method[8]

range or not. If both signal strengths lie or do not lie in the visibility threshold range then there will be no penalty for these patches and their signal strengths are referred to as significant but if any one of them lies in visibility threshold range and another one does not lie in visibility threshold range then these patches would be penalized and their signal strengths are referred to as insignificant.

We use nonlinear mapping to discriminate between significant and insignificant signal strengths. It maps the most insignificant signal strength to 0 and most significant signal strength to 1 and it smoothly varies in-between.
We can calculate our local structural fidelity measure using following equation[8]:

$$S_{local}(x,y) = \frac{2\sigma_x^{'}\sigma_y^{'} + C_1}{\sigma_x^{'2} + \sigma_y^{'2} + C_1} \cdot \frac{\sigma_{xy} + C_2}{\sigma_x\sigma_y + C_2} \tag{2.19}$$

Here, x is HDR local patch and y is its corresponding LDR local patch. Also, σ_x, σ_y and σ_{xy} are two standard deviations and one cross correlation between HDR local patch and LDR local patch respectively. We have used C_1 and C_2 as a positive stabilization constants. Moreover, $\sigma^{'}$ is the modified value of local standard deviation σ which can be obtained by passing through a nonlinear mapping. The relationship

Figure 2.11: An image pyramid structure[8]

between σ and $\sigma^{'}$ can be given by following equation[8]:

$$\sigma^{'} = \frac{1}{\sqrt{2\pi\theta_\sigma}} \int_{-\infty}^{\sigma} exp - \left[\frac{(x-\tau_\sigma)^2}{2\theta_\sigma^2} \right] dx \tag{2.20}$$

As the ability of single scale method is limited, we use a multi scale approach. In it, images are passed through low pass filters and down samplers to generate an image pyramid structure. The overall frame work has been shown in figure 2.10 and image pyramid structure has been shown in figure 2.11. The overall single score can be achieved by averaging all single scores at each scale by[8]:

$$S_l = \frac{1}{N_1} \sum_{i=1}^{N_l} S_{local}(x_i, y_i) \tag{2.21}$$

Here, x_i and y_i are i^{th} local patches from HDR image and the tone mapped LDR image respectively. N_l is total number of patches in l^{th}scale. Therefore, the value of SSIM measure will be between range of 0 and 1.

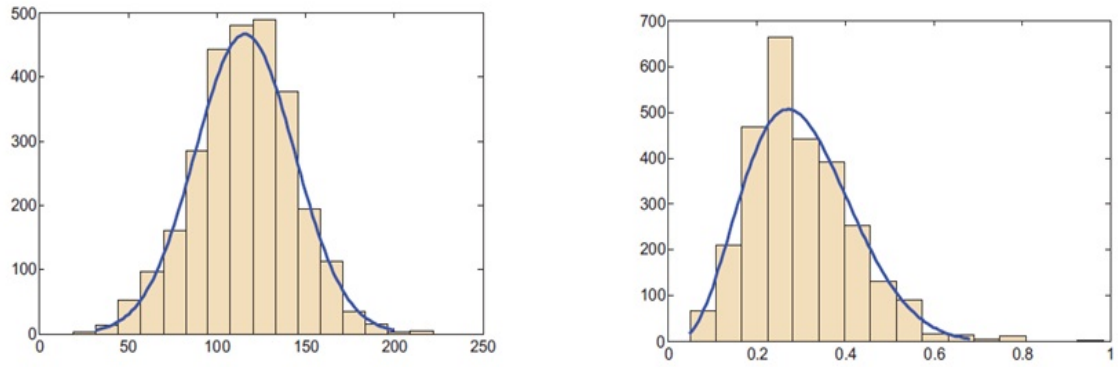

Figure 2.12: Histograms of (a) means and (b) standard deviations of natural images[8]

NSS: Naturalness of an image cannot be easily defined quantitatively. From a literature survey of biological vision and image processing applications, it has been analyzed that image brightness and image contrast play a major role in maintaining naturalness in an image. These two characteristics can be reflected from images mean and standard deviations. The dataset of 3000 8 bits/pixel gray-scale natural scene images has been used to generate the histograms of the means and standard deviations of these images which can be shown in figure 2.12.

The area of these histograms can be covered by following equations[8]:

$$P_m(m) = \frac{1}{\sqrt{2\pi\sigma_m}}\, exp\left[- \frac{m - \mu_m}{2\sigma_m^2} \right] \tag{2.22}$$

$$P_d(d) = \frac{(1-d)^{\beta_d - 1} d^{\alpha_d - 1}}{B(\alpha_d, \beta_d)} \tag{2.23}$$

Here, we have used a Gaussian and a Beta functions to cover the area of histograms. As brightness and contrast work independently and do not depend on each other with respect to natural image statistics as well as biological computation, their joint probability density function(PDF) can be given by product of their individual PDFs. So, the statistical naturalness measure can be given by[8],

$$N = \frac{1}{K} P_m P_d \tag{2.24}$$

Here, $K$is a normalization factor which can be found by $K = max\{P_m P_d\}$. Therefore, value of statistical naturalness will be between 0 and 1.

TMQI: As naturalness is related to the dynamic range of an image, human observer may not be able to differentiate naturalness measure between HDR and its tone mapped LDR image. It makes clear that structural fidelity measurement (SSIM) plays a major role than naturalness measurement (NSS). These measurement values can be used individually or they can also be used as a vector quantity. In a practical scenario, a single score is desired to rate the overall quality of an image. This requirement can be fulfilled using tone mapped image quality index (TMQI) measure which uses both SSIM and NSS measurements and return just one single score.

Such tone mapped image quality index using three different adjustment parameters can be given by[8],

$$Q = aS^{\alpha} + (1 - a)N^{\beta} \tag{2.25}$$

Here, the value of a reflects the importance of SSIM and NSS with respect to each other where a can be from range [0,1]. S and N are the measurements computed based on SSIM and NSS algorithms respectively. Moreover, α and β decide the sensitivities of SSIM and NSS respectively. As values of S ,Q and N are bound to range [0,1].

2.4.2.3 Algorithm Implementation

As we discussed, each tone mapping operator which uses logarithmic scaling property accommodate different kind of deficiencies. Using contrast-limited adaptive histogram equalization, we can maintain a perceptual equivalence between our HDR and LDR images [5]. HDR data represents the amount of light captured from any scene and it does not reflect just colors of an image. As our eyes would do, wards tone mapping algorithm takes logarithm of these light values which helps us in increasing contrast of our image when using histogram equalization with it. In this process, it makes use of the overall dynamic range available and due to that it would be able to restore the contrast and saturation lost by logarithmic luminance compression. On the basis

of wards visibility matching tone mapping operator [5], we have implemented a tone mapping algorithm here. It takes .hdr image file as input and returns .jpg image file as output. It applies the inverse gamma correction to input image. The basic steps of wards tone mapping operator can be seen in figure 2.13:

2.5 Summary

This chapter builds basis of our thesis as it gives a brief introduction of all important terms used in it and explores two important algorithms used in HDR imaging. Firstly, it discusses the structure and working of human eye and digital camera from references [1] and [2]. It has also compared their working with respect to their dynamic ranges. As color space conversion process play an important role in HDR imaging, we have studied two possible methods for it from references [3] and [4]. Then, we have studied two important algorithms for HDR imaging: dynamic range expansion using differently exposed images and dynamic range compression (tone mapping). This study starts from their theoretical perspective and move to their mathematical as well as implementation process flow. We have also covered three assessment methods for tone mapping operator: Modified SSIM, NSS and TMQI.

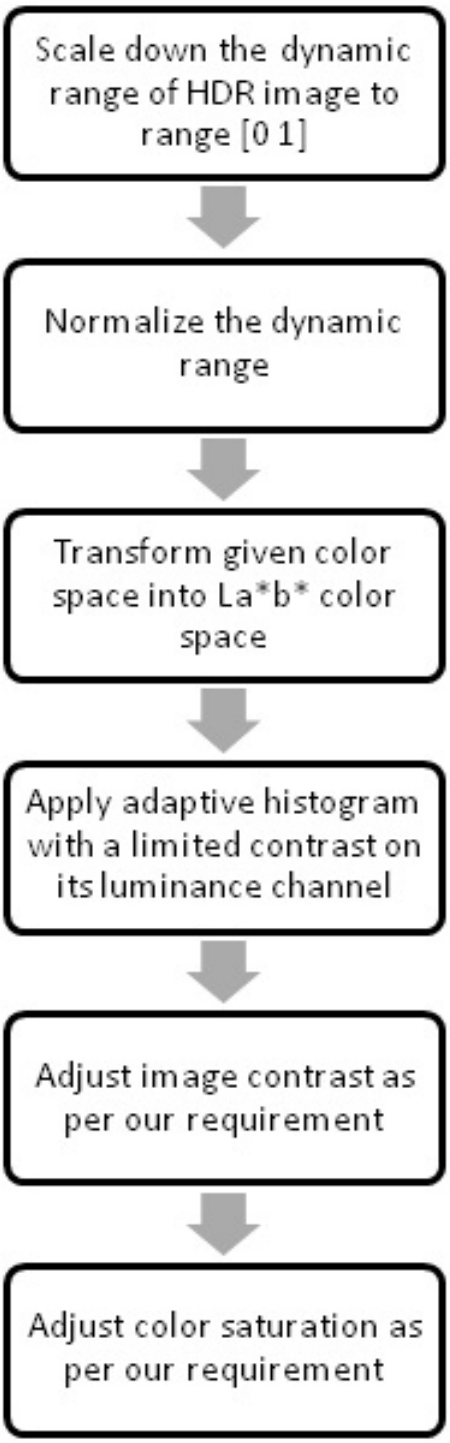

Figure 2.13: Wards visibility matching TMO process flow [5]

Chapter 3

Proposed Algorithm

3.1 Introduction

In the last chapter, we have seen implementation process of two algorithms: dynamic range expansion using differently exposed images and dynamic range compression (tone mapping). We use these two algorithms in a cascaded manner i.e. output of first algorithm was given to the input of second algorithm. Therefore, the overall algorithm takes differently exposed images and their corresponding exposure timings as input and gives a tone mapped HDR image in output. The general HDR imaging pipeline has been shown in figure 3.1.

Normally, we use same TMO for all scenes to be captured. As we know, performance

Figure 3.1: The Overall Algorithm

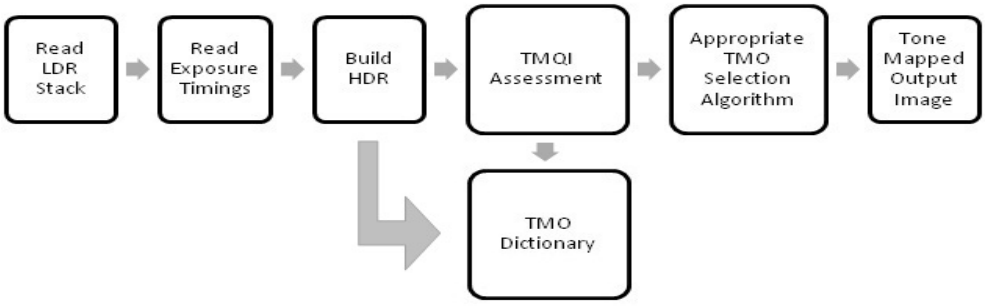

Figure 3.2: The Overall Algorithm

of TMO varies with scene and that is why to optimize the performance of our algorithm, we should use the best possible TMO according to the scene to be captured. Based on this idea, we have designed our algorithm that maintains a dictionary of TMOs and selects the best one according to present scene to be captured. Currently we have maintained five TMOs in our dictionary: DragoTMO, GammaTMO, LogarithmicTMO, ReinhardTMO and WardHistAdjTMO. We can also maintain more TMOs in dictionary. The proposed algorithm has been shown in figure 3.2.
If we compare 3.1 and 3.2, we can observe that one block of general algorithm has been replaced by two blocks in proposed algorithm. The first block is dictionary of TMOs and the second one is decision making block. These two blocks plays a major role in our proposed algorithm. They maintain a proper list of TMO and selects the best possible according to the present scen to be captured. The results of our proposed algorithm will be discussed in next chapter.

3.2 Summary

This chapter introduces our proposed algorithm and discusses its importance. Moreover, it also discusses the block diagram of our proposed algorithm.

Chapter 4

Simulation Results & Assessment

Our database consists of total eighteen datasets taken from references [17], [18], [13], [14],[15] and [16]. Images of all datasets have been shown in figures 4.1, 4.2 and 4.3. Exposure details of datasets (o) and (p) are shown in tables I and II. All algorithms were implemented on an Intel Core 2 Duo 2.20GHz CPU with 3GB RAM.

4.1 Basic HDR imaging pipeline

In chapter 2, we have studied and understood implementation process of two algorithms: dynamic range expansion using differently exposed images and dynamic range compression (tone mapping). First algorithm takes differently exposed images and their corresponding exposure timings as input and returns an HDR image in output. Whereas second algorithm takes an HDR image as input and gives an LDR image in output. In this chapter, we used these two algorithms in a cascaded manner i.e. output of first algorithm was given to the input of second algorithm. Therefore, the basic HDR imaging pipeline takes differently exposed images and their corresponding exposure timings as input and gives a tone mapped HDR image in output. The differently exposed LDR images, tone mapped HDR output image and corresponding exposure timings for dataset (o) are shown in figure 4.4 and table I respectively. The tone mapped HDR output image scored 0.8751 out of 1 on scale of Q score.

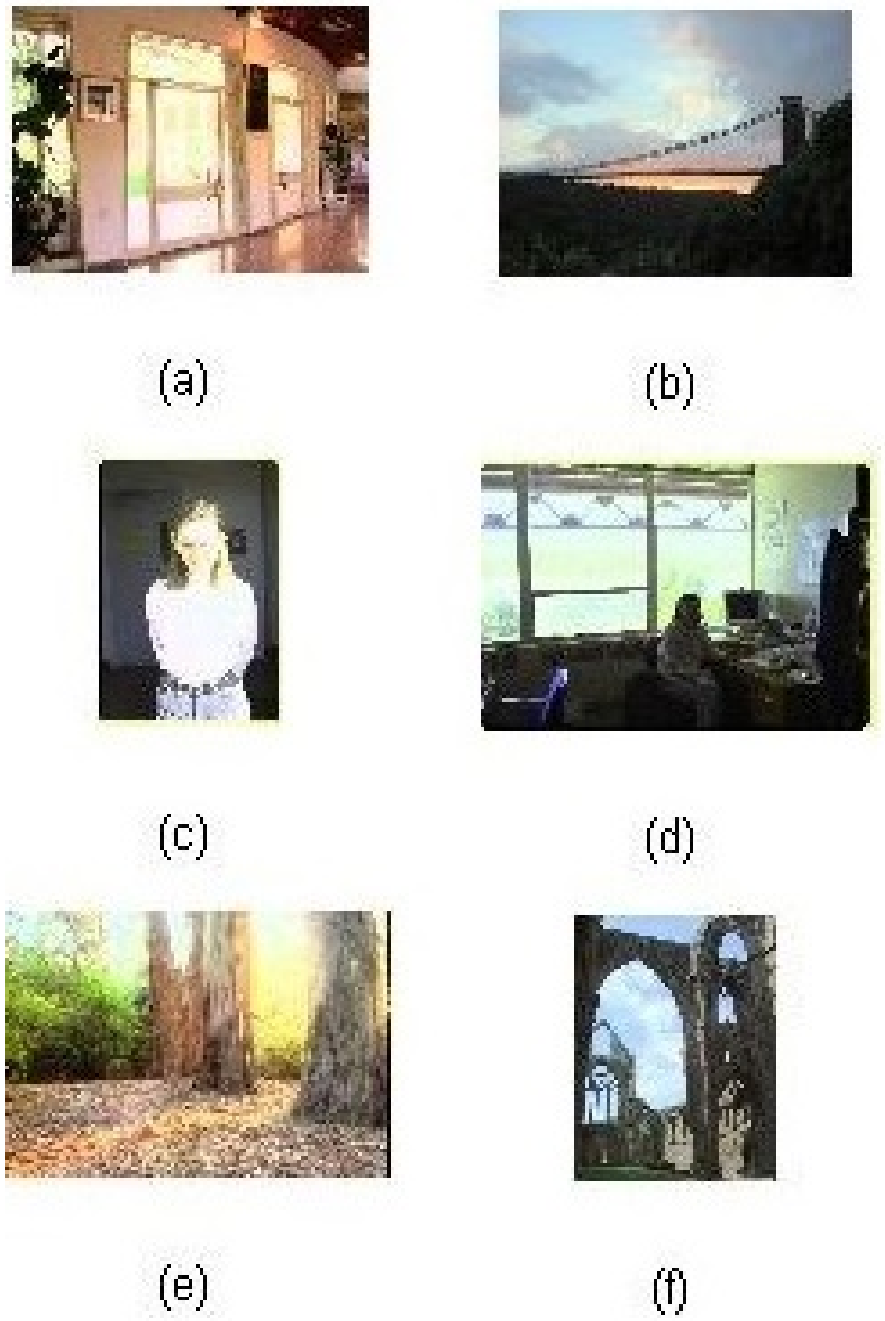

Figure 4.1: Database

Figure 4.2: Database

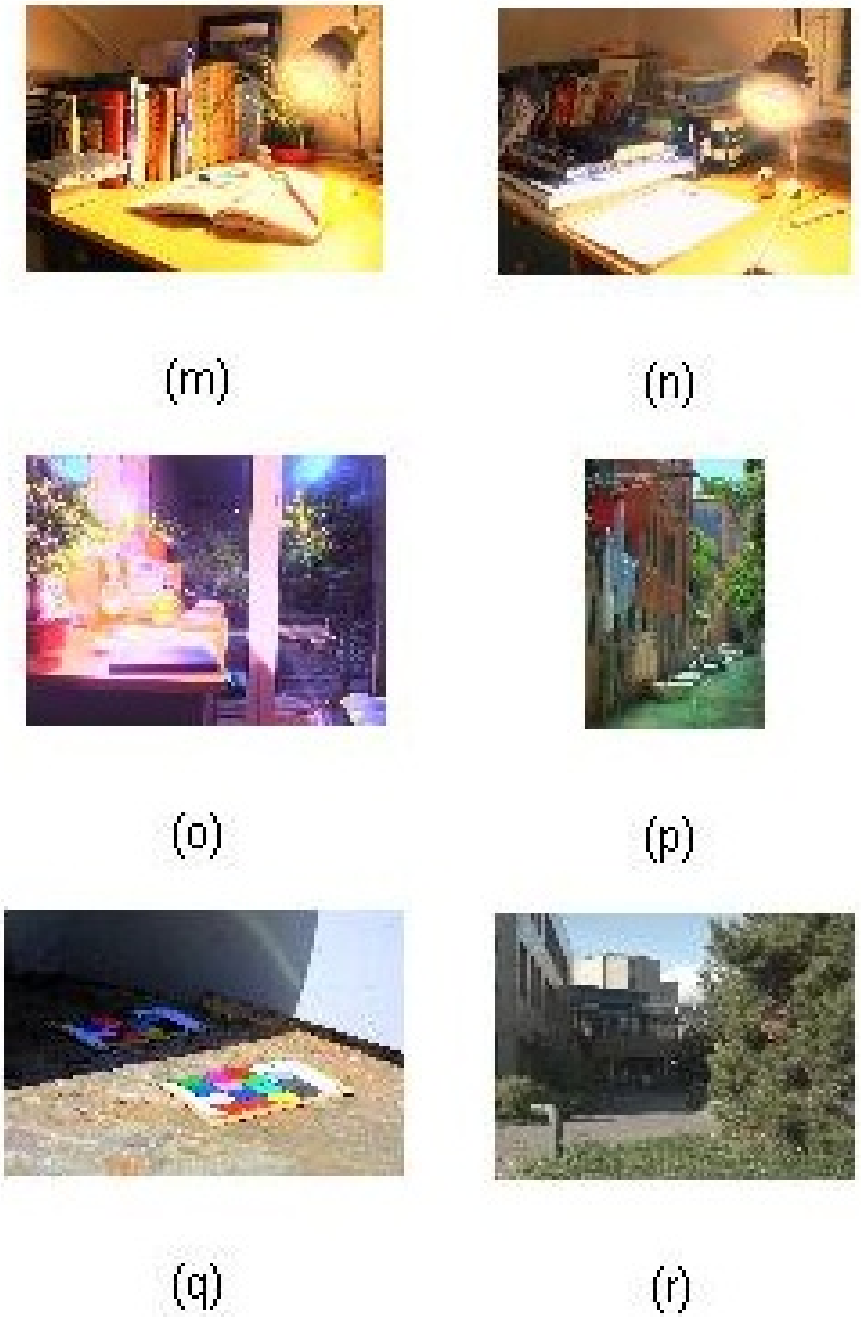

Figure 4.3: Database

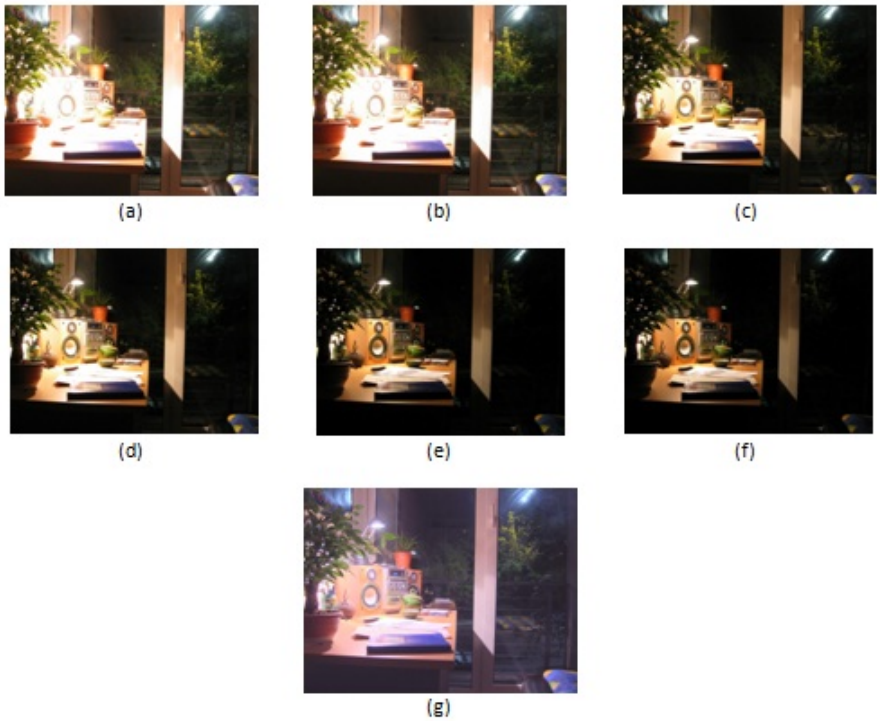

Figure 4.4: Dataset 1: LDR images and Tone mapped HDR output image

Table I: Exposure timings of dataset (o) [18]

LDR input image number (j)	**Corresponding exposure time** (Δt_j)
1	4.000
2	3.200
3	1.000
4	0.800
5	0.300
6	0.250

Similarly, the differently exposed LDR images, tone mapped HDR output image and corresponding exposure timings for dataset (p) are shown in figure 4.5 and table II respectively. The tone mapped HDR output image scored 0.9335 out of 1 on the scale of Q score.

Figure 4.5: Dataset 2: LDR images and Tone mapped HDR output image

Table II: Exposure timings of dataset (p) [17]

LDR input image number (j)	Corresponding exposure time (Δt_j)
1	0.0500000
2	0.0125000
3	0.0031250

4.2 Proposed Algorithm

In chapter 3, we have introduced our proposed algorithm and discussed its block diagram. We have maintained eight TMOs in our dictionary which are enlisted in table III[6]. We apply these TMOs over eighteen datasets and evaluate their performance by analyzing their average scores by two image quality assessment methods:

Objective Assessment: In it, we assess them based on their scores given by TMQI algorithm.

Subjective Assessment: In it, we assess them based on their scores given by twenty subjects on the scale of five.

Surveys of objective and subjective assessments have been given in table V and VI respectively. We have highlighted highest scores for each database in both tables. Moreover, we have also enlisted average scores of each TMO in both surveys.

Matching of highest average scores in both survey shows reliability of our proposed algorithm.So, the highest Q scored TMO will be selected to generate output. The frequency of each TMO to be used for generating output is shown in table IV which clears that TMO_8 is more reliable than other TMOs. Final tone mapped HDR output images for all TMOs have been shown in figures 4.6 to 4.23.

Table III: List of TMOs[6]

TMO_No	**TMO_Name**
TMO_1	DragoTMO
TMO_2	GammaTMO
TMO_3	LogarithmicTMO
TMO_4	ReinhardTMO
TMO_5	WardHistAdjTMO
TMO_6	KimKautzConsistentTMO
TMO_7	ChiuTMO
TMO_8	ExponentialTMO

Table IV: Number of Times TMO used for output

TMO_No	**No of times used for generating output**
TMO_1	6
TMO_2	2
TMO_3	1
TMO_4	0
TMO_5	0
TMO_6	2
TMO_7	0
TMO_8	7

Table V: Objective Q score survey

	TMO_1	**TMO_2**	**TMO_3**	**TMO_4**	**TMO_5**	**TMO_6**	**TMO_7**	**TMO_8**
Dataset_a	0.828063781	0.729287367	0.583874208	0.789485625	0.774074873	0.790284203	0.751559681	**0.867216533**
Dataset_b	**0.854937677**	0.796701486	0.698288728	0.788115909	0.76533795	0.84728304	0.703862934	0.748387454
Dataset_c	0.696627076	0.733079452	0.754777762	0.754894218	0.737460361	0.760617517	0.725796101	**0.898664376**
Dataset_d	0.809483521	0.891086683	0.733492147	0.803425242	0.773962847	0.777838249	0.730797345	**0.905521216**
Dataset_e	0.782892859	0.865605445	0.752124101	0.802638135	0.788435748	0.827807002	0.777474211	**0.865748321**
Dataset_f	**0.977878227**	0.804689747	0.795870492	0.82065103	0.805370307	0.844076664	0.76429366	0.898529315
Dataset_g	**0.936790807**	0.820445094	0.639049466	0.788849575	0.782128701	0.785045234	0.775928997	0.856301724
Dataset_h	0.84025784	0.763087428	0.630279264	0.812913534	0.799090573	**0.853820269**	0.765274474	0.810056014
Dataset_i	**0.924691516**	0.791959745	0.72850255	0.78676092	0.75266374	0.815312688	0.718427355	0.887241166
Dataset_j	0.832795486	**0.893239335**	0.691636896	0.767405337	0.757527107	0.772660868	0.723779252	0.868084552
Dataset_k	**0.926721312**	0.821383072	0.666711644	0.766852328	0.761457228	0.810168758	0.759351237	0.879459927
Dataset_l	**0.947666415**	0.824468515	0.76827293	0.804200357	0.789049103	0.813045181	0.745288125	0.865796894
Dataset_m	0.698992414	0.708262438	0.759030121	0.791404728	0.777565443	0.798754057	0.740185006	**0.910168639**
Dataset_n	0.688656041	0.700293328	0.739526423	0.760015262	0.758718946	0.774702819	0.720117295	**0.895400113**
Dataset_o	0.854314653	0.743160017	0.636487501	0.751518144	0.752027502	0.75474083	0.726549029	**0.908245048**
Dataset_p	0.346776414	0.356900259	**0.934798294**	0.798435388	0.802845595	0.803839577	0.778316021	0.872626827
Dataset_q	0.850018164	0.866953765	0.765653781	0.790480293	0.791342974	**0.881252759**	0.720642145	0.754482928
Dataset_r	0.925948431	**0.954687917**	0.823237532	0.819653203	0.811776913	0.891670754	0.764752726	0.859080764
Minimum Q score	0.346776414	0.356900259	0.583874208	0.751518144	0.737460361	0.75474083	0.703862934	0.748387454
Maximum Q score	0.977878227	0.954687917	0.934798294	0.82065103	0.811776913	0.891670754	0.778316021	0.910168639
Average Q score	0.817972924	0.781405061	0.727867436	0.788761068	0.776713106	0.811273359	0.744021978	**0.863945101**

Table VI: Subjective Q score survey

	TMO_1	**TMO_2**	**TMO_3**	**TMO_4**	**TMO_5**	**TMO_6**	**TMO_7**	**TMO_8**
Dataset_a	3.592416	1.347156	0.898104	2.24526	2.694312	4.041468	3.592416	**4.49052**
Dataset_b	**4.49052**	2.24526	0.898104	2.694312	3.143364	3.592416	1.796208	2.694312
Dataset_c	0.898104	0.898104	1.796208	2.24526	2.0656392	2.694312	1.8860184	**4.49052**
Dataset_d	4.041468	3.592416	1.796208	1.6165872	0.898104	1.347156	1.0777248	**4.49052**
Dataset_e	3.592416	4.041468	1.347156	0.898104	1.796208	3.143364	2.694312	**4.49052**
Dataset_f	**4.49052**	0.898104	1.796208	2.694312	3.143364	3.592416	2.24526	4.041468
Dataset_g	**4.49052**	2.694312	0.898104	2.24526	3.592416	1.347156	1.796208	4.041468
Dataset_h	3.592416	2.694312	2.24526	2.7841224	2.6045016	**4.49052**	2.5146912	2.694312
Dataset_i	**4.49052**	2.694312	2.5146912	2.6045016	2.469786	3.143364	0.898104	2.8739328
Dataset_j	2.8739328	**4.49052**	0.898104	2.5146912	2.4248808	2.4248808	1.9758288	2.9637432
Dataset_k	**4.49052**	3.4127952	0.898104	2.9637432	2.9637432	3.3229848	2.6045016	3.5026056
Dataset_l	**4.49052**	3.7720368	3.4127952	3.592416	3.3229848	3.6822264	0.898104	3.9516576
Dataset_m	0.898104	1.796208	1.9758288	2.24526	2.1554496	2.4248808	1.8860184	**4.49052**
Dataset_n	0.898104	1.796208	1.9758288	2.24526	2.1554496	2.4248808	1.8860184	**4.49052**
Dataset_o	4.041468	2.5146912	0.898104	2.6045016	2.6045016	2.6045016	2.24526	**4.49052**
Dataset_p	0.898104	1.347156	**4.49052**	2.24526	2.3350704	2.4248808	2.0656392	2.9637432
Dataset_q	3.6822264	3.592416	4.1312784	3.4127952	3.5026056	**4.49052**	0.898104	2.24526
Dataset_r	4.041468	**4.49052**	3.3229848	3.2331744	3.143364	3.2331744	0.898104	2.8739328
Minimum Q score	0.898104	0.898104	0.898104	0.898104	0.898104	1.347156	0.898104	2.24526
Maximum Q score	4.49052	4.49052	4.49052	3.592416	3.592416	4.49052	3.592416	4.49052
Average Q score	3.332963733	2.684333067	2.010755067	2.504712267	2.6119858	3.0236168	1.881028933	**3.6822264**

Figure 4.6: Dataset a : Outputs of TMO (1) to (8) : (a) to (h) respectively

Figure 4.7: Dataset b : Outputs of TMO (1) to (8) : (a) to (h) respectively

Figure 4.8: Dataset c : Outputs of TMO (1) to (8) : (a) to (h) respectively

Figure 4.9: Dataset d : Outputs of TMO (1) to (8) : (a) to (h) respectively

Figure 4.10: Dataset e : Outputs of TMO (1) to (8) : (a) to (h) respectively

Figure 4.11: Dataset f : Outputs of TMO (1) to (8) : (a) to (h) respectively

Figure 4.12: Dataset g : Outputs of TMO (1) to (8) : (a) to (h) respectively

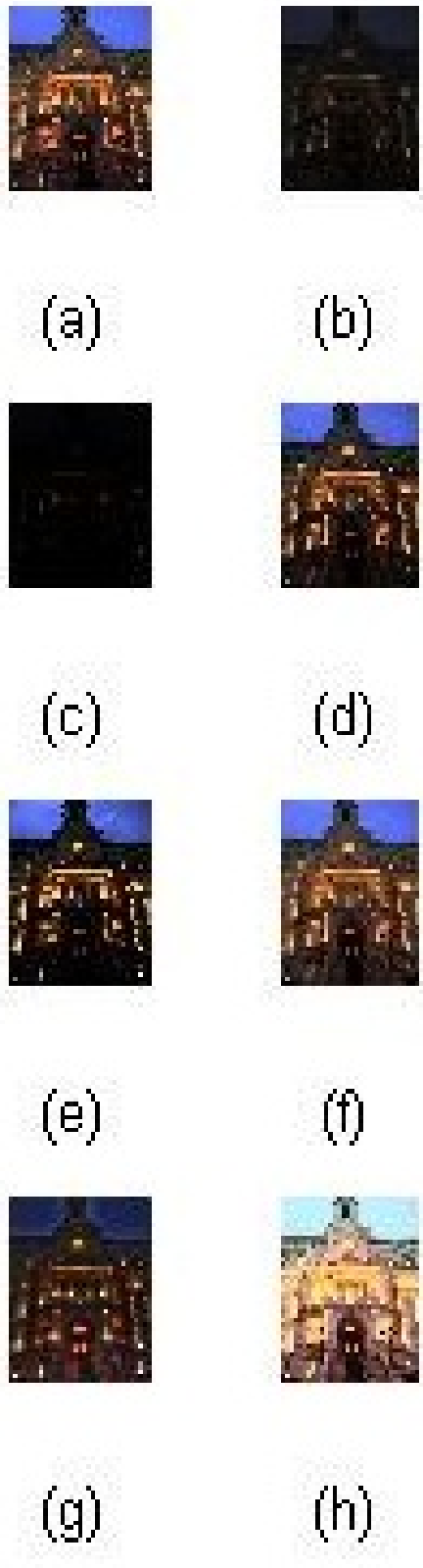

Figure 4.13: Dataset h : Outputs of TMO (1) to (8) : (a) to (h) respectively

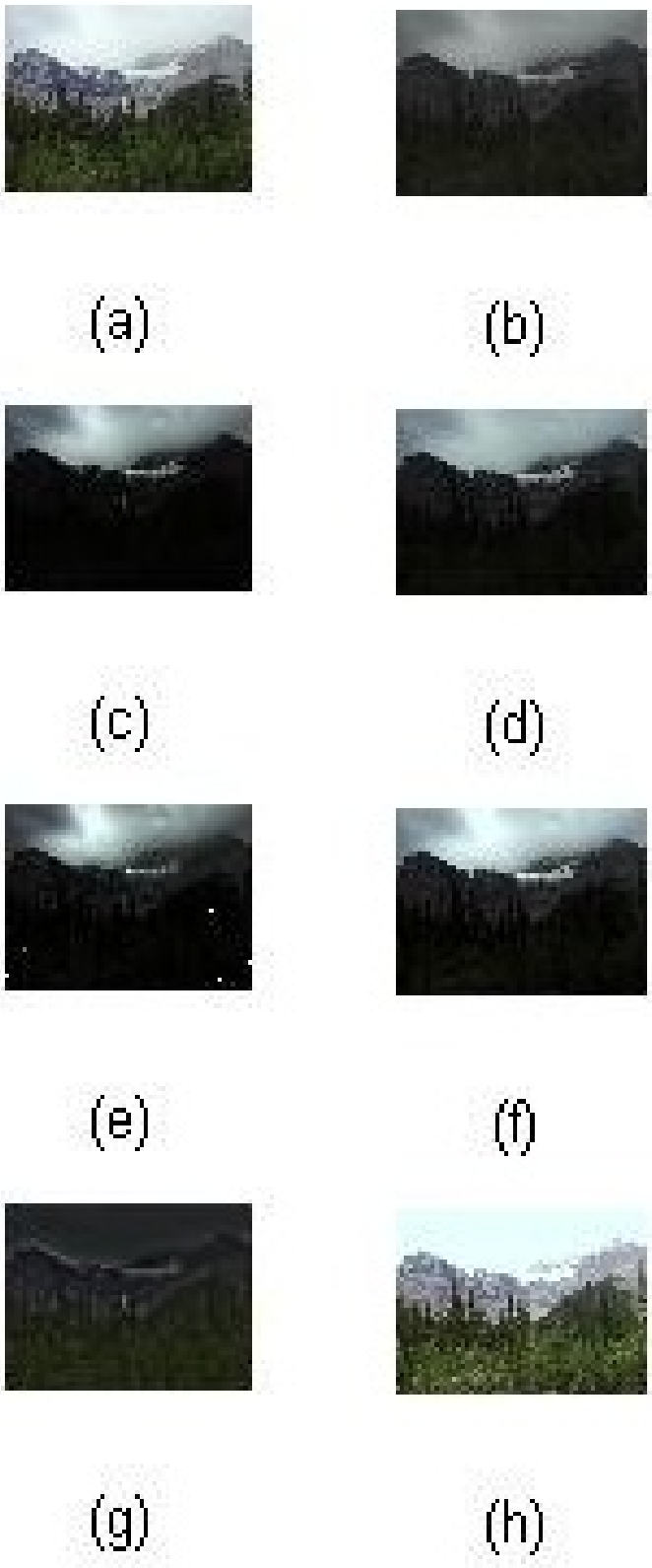

Figure 4.14: Dataset i : Outputs of TMO (1) to (8) : (a) to (h) respectively

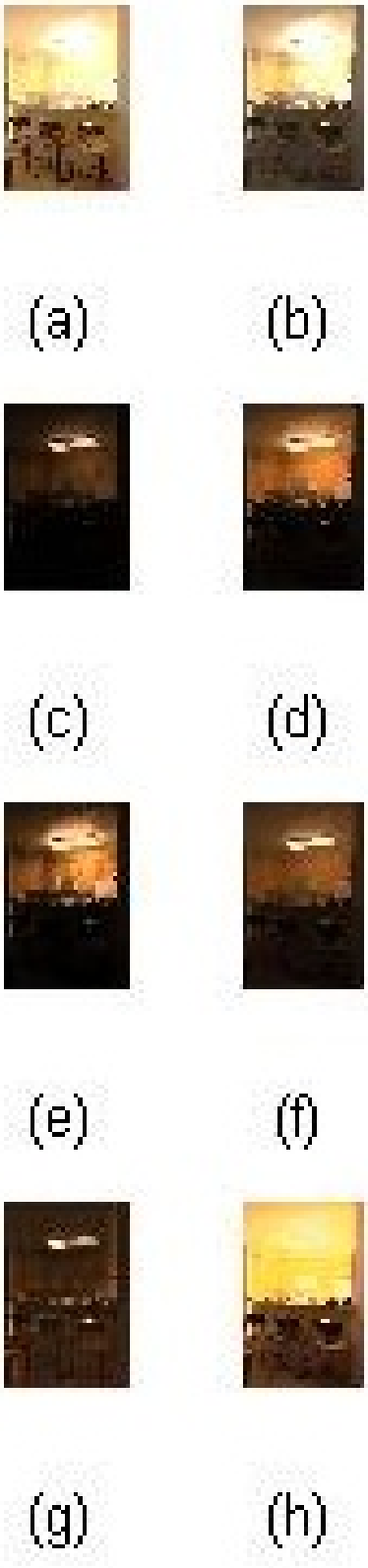

Figure 4.15: Dataset j : Outputs of TMO (1) to (8) : (a) to (h) respectively

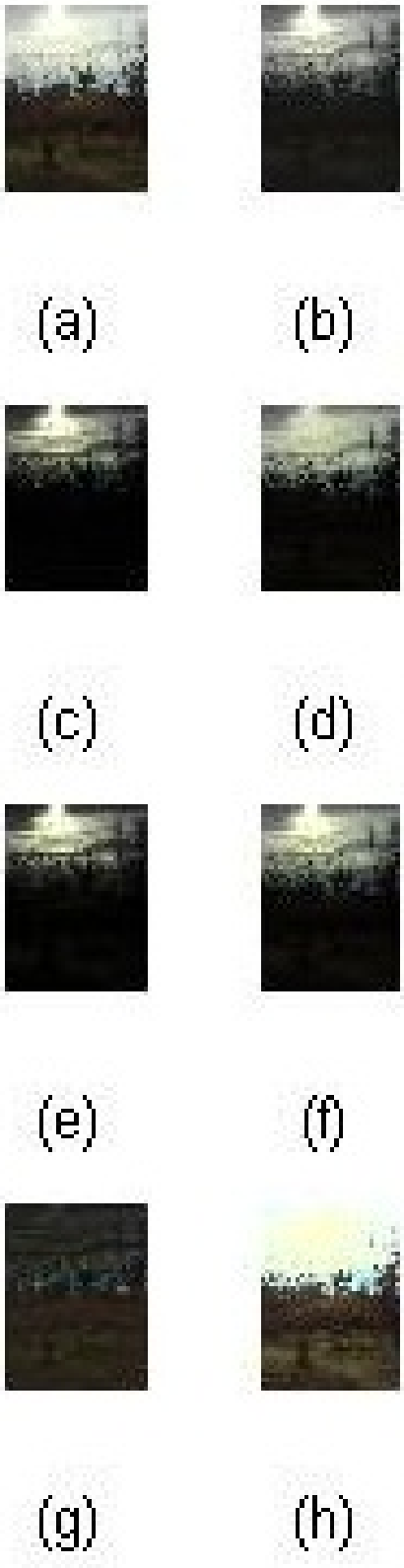

Figure 4.16: Dataset k : Outputs of TMO (1) to (8) : (a) to (h) respectively

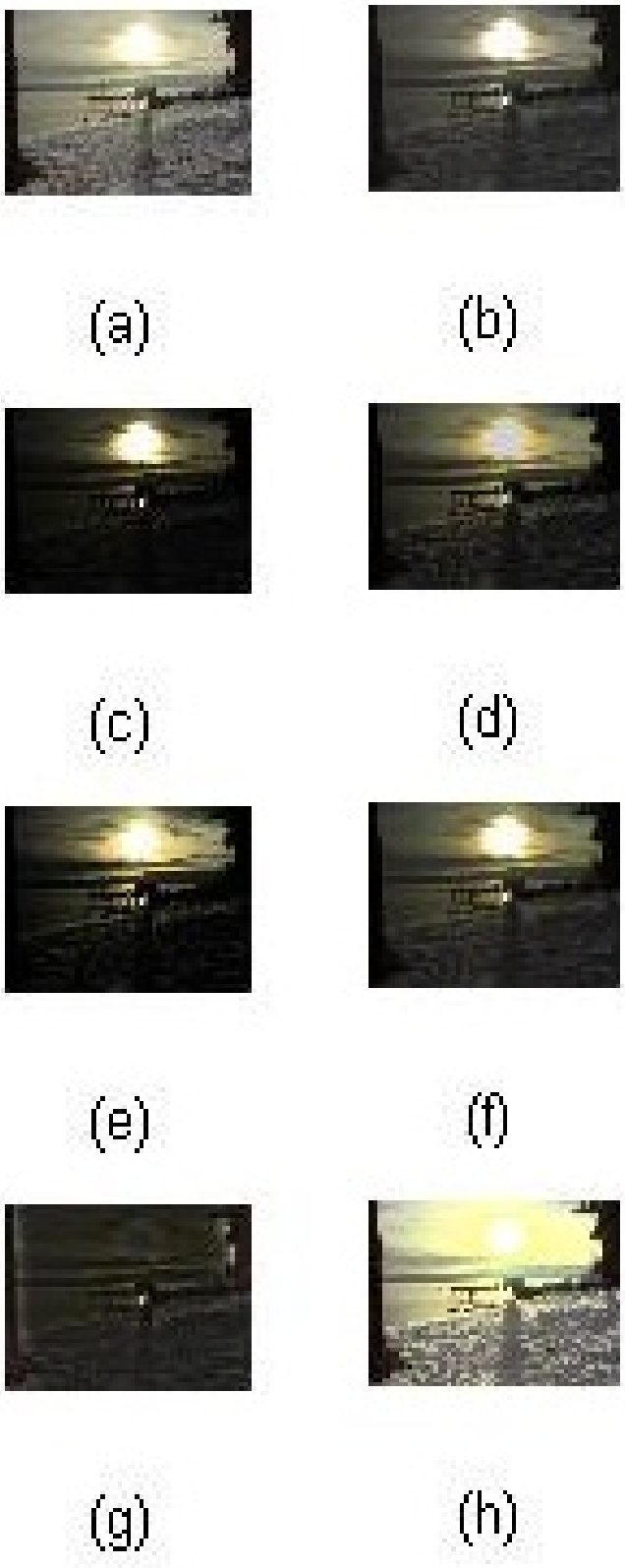

Figure 4.17: Dataset l : Outputs of TMO (1) to (8) : (a) to (h) respectively

Figure 4.18: Dataset m : Outputs of TMO (1) to (8) : (a) to (h) respectively

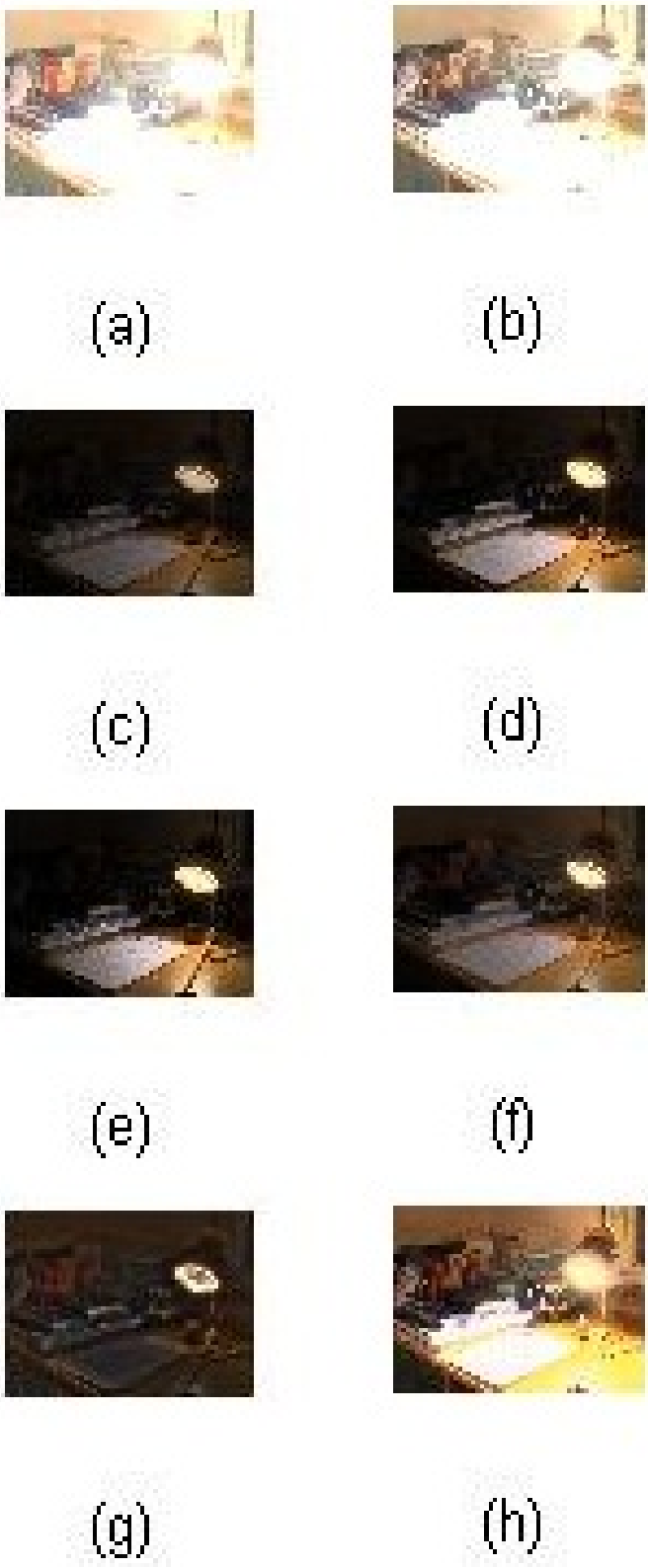

Figure 4.19: Dataset n : Outputs of TMO (1) to (8) : (a) to (h) respectively

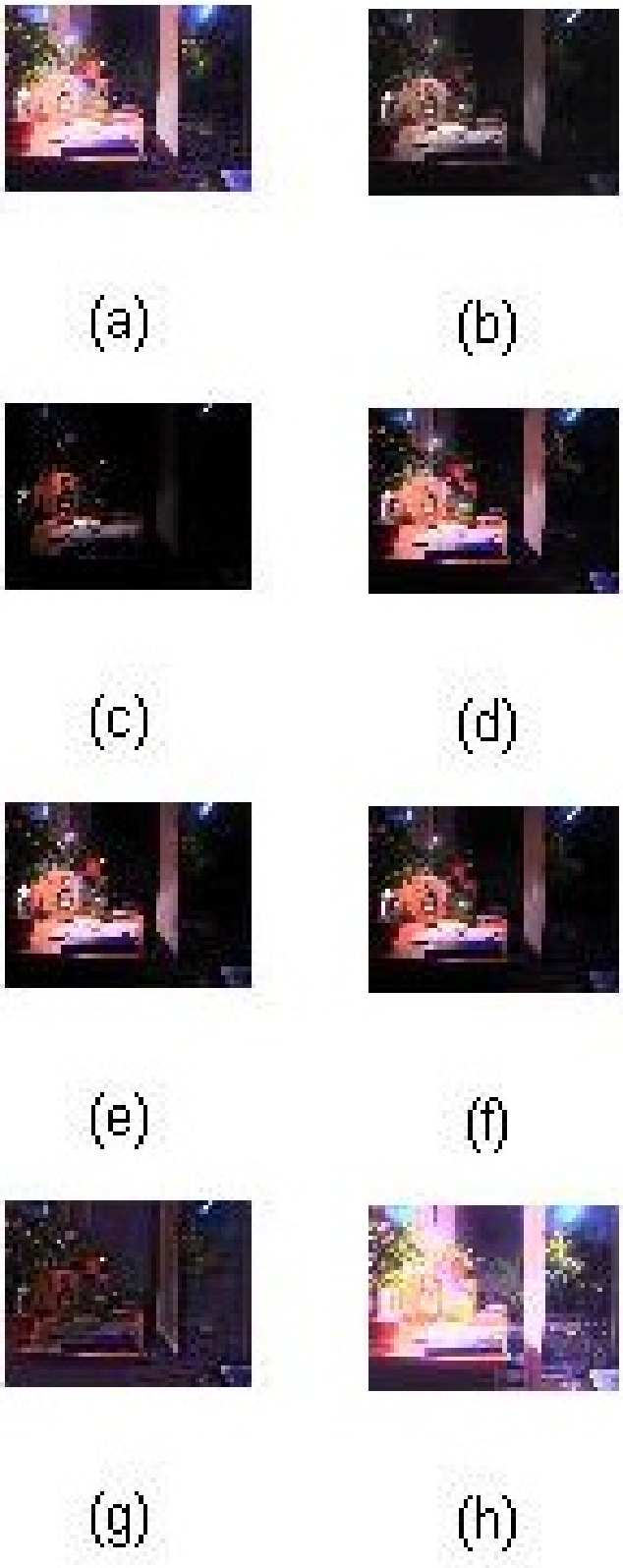

Figure 4.20: Dataset o : Outputs of TMO (1) to (8) : (a) to (h) respectively

Figure 4.21: Dataset p : Outputs of TMO (1) to (8) : (a) to (h) respectively

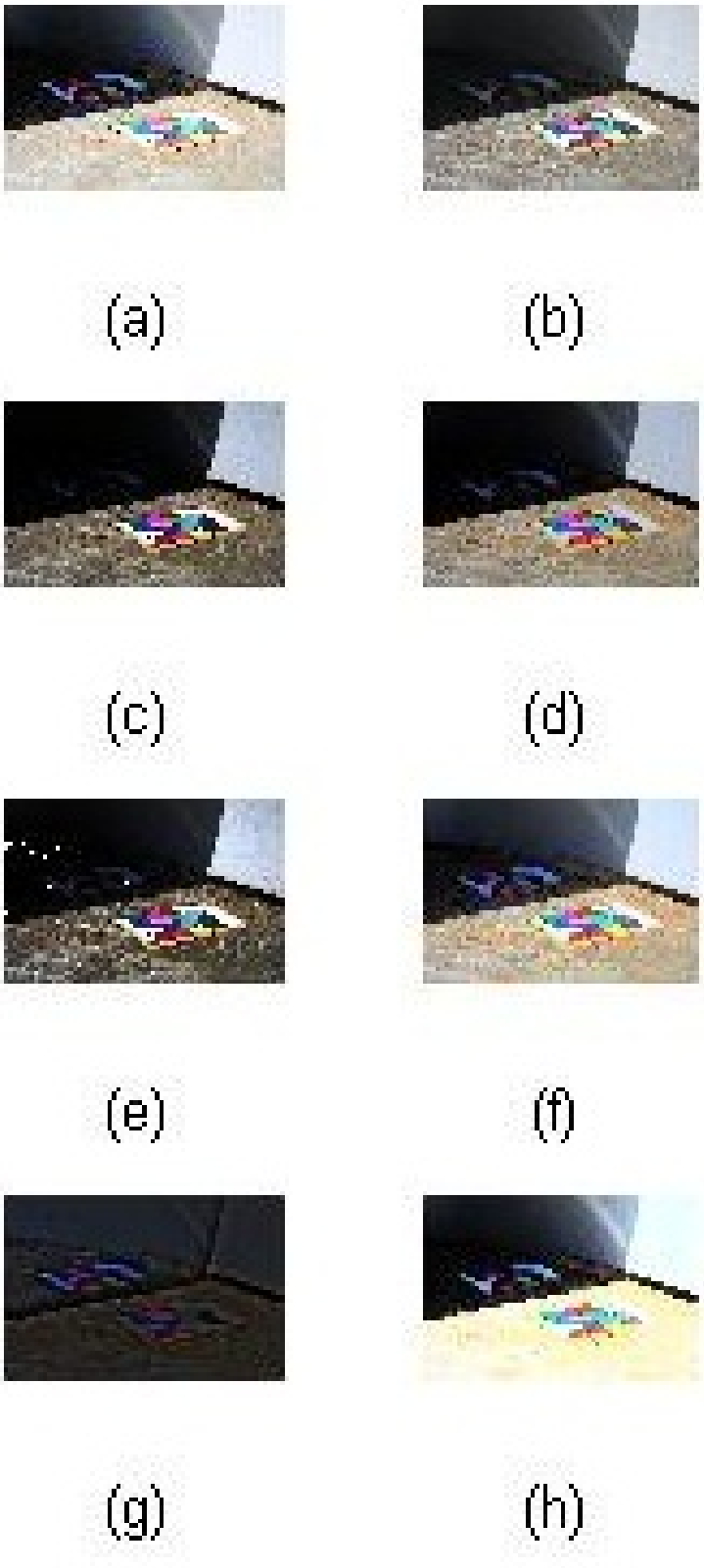

Figure 4.22: Dataset q : Outputs of TMO (1) to (8) : (a) to (h) respectively

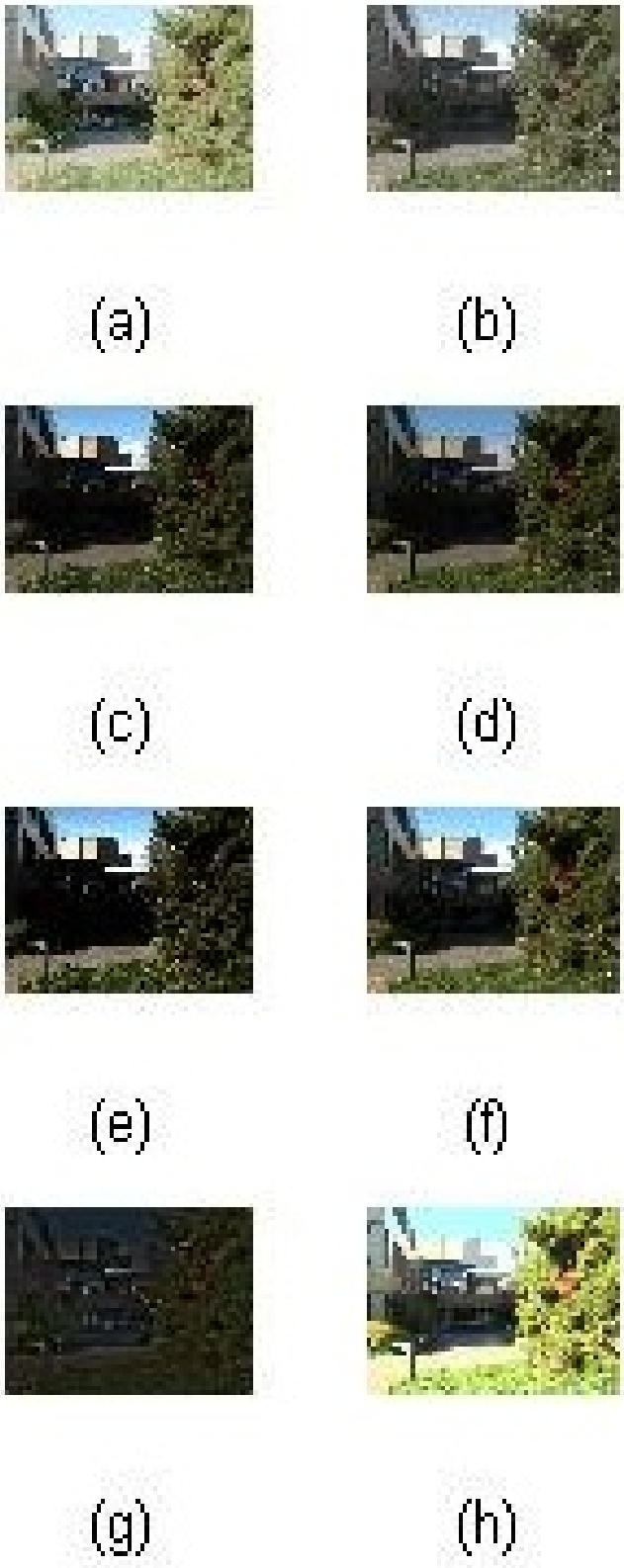

Figure 4.23: Dataset r : Outputs of TMO (1) to (8) : (a) to (h) respectively

4.3 Summary

In this chapter, we have analyzed working of algorithms discussed in chapter 2 and chapter 3 based on their inputs and outputs. We have also assessed their performance by assessing their output with help objective and subjective image quality assessment methods. Moreover, we took fourteen datasets from references [13], [14],[15] and [16] and compared performances of eight tone mapping operators. These surveys illustrated the capability of TMQI algorithm to evaluate the performance of any TMO in our proposed algorithm.

Chapter 5

Conclusion & Future Scopes

5.1 Conclusion

The dynamic range used in general purpose imaging devices has limitations which restrict us from capturing realistic scene information present in low as well as high intensity areas. We studied and implemented HDR imaging pipeline which solves this problem. As discussed in thesis, TMQI algorithm is one of the best methods to evaluate HDR imaging algorithm generated resultant image. Moreover, the capability of TMQI algorithm has been demonstrated by applying eight TMOs on HDR images of eighteen datasets.

As there are many TMOs available for use, we have proposed an algorithm which helps in selecting appropriate TMO from a maintained TMO dictionary for any particular scene to be captured. The working and importance of our proposed algorithm of our proposed algorithm have also been shown with help of results and their assessment.

5.2 Future Scope

The weighting function used in HDR imaging pipeline can be fixed or adaptive. We have considered fixed weighting function in this thesis. We can also design an adaptive weighting function which changes itself with respect to the scene to be captured.

Moreover, we have used TMQI algorithm to select appropriate TMO for any scene to be captured. Moreover, we can also consider it to optimize performance of any TMO. Lastly, we can try to reduce the simulation time of our proposed algorithm.

References

[1] R. C. Gonzalez and R. E. Woods, "*Digital Image Processing*", Prentice Hall, 2008.

[2] Gaurav Sharma, "*Digital Color Imaging Handbook*", CRC Press, 2003.

[3] Christian Bloch, "*The HDRI Handbook 2.0: High Dynamic Range Imaging for Photographers and CG Artists*", Rocky Nook, 2007.

[4] Erik Reinhard, Greg Ward, Paul Debevec, Sumanta Pattanaik, Wolfgang Heidrich, and Karol Myszkowski, "*High Dynamic Range Imaging: Acquisition, Display, and Image Based Lighting*", Morgan Kaufmann Publishers, San Francisco, 2010.

[5] G. W. Larson, H. Rushmeier, and C. Piatko, "*A visibility matching tone reproduction operator for high dynamic range scenes,*" in *IEEE Trans. Visual. Comput. Graph.*, vol. 3, no. 4, pp. 291306, Oct.Dec. 1997.

[6] Francesco Banterle, Alessandro Artusi, Kurt Debattista, and Alan Chalmers, "*Advanced High Dynamic Range Imaging: Theory and Practice*", CRC Press, 2011.

[7] P. E. Debevec, and J. Malik, "*Recovering High Dynamic Range Radiance Maps from Photographs,*" in *Proceedings of SIGGRAPH97*, Computer Graphics Proceedings, Annual Conference Series, pp. 369378, August 1997.

[8] Hojatollah Yeganeh, and Zhou Wang, "*Objective Quality Assessment of Tone-Mapped Images,*" in "*IEEE Trans. Image Process.*, vol.22, no.2, pp. 657-668, Feb 2013.

[9] S. Mann, and R.W. Picard., "*Being Undigital with Digital Cameras: Extending Dynamic Range by Combining Differently Exposed Pictures,*" in *IS&Ts 48th Annual Conference*, pp. 422428, Springfield, VA, 1995.

[10] Z. Wang, E. P. Simoncelli, and A. C. Bovik., "*Multi-scale structural similarity for image quality assessment,*" in *Proc. IEEE Asilomar Conf. Signals*, Syst., Comput., Pacific Grove, CA, Nov. 2003, pp. 13981402.

[11] Y. Bandoh, G. Qiu, M. Okuda, S. Daly, T. Ach, and O. C. Au, "*Recent advance in high dynamic range imaging technology,*" in *IEEE 17th International Conference*, on Intelligent and Advanced Systems (ICIAS2012), International Conference on Image Processing September, 2010, pp. 3125-3128.

[12] Venkata Lakshmi, S., Sujatha, S., Janet J., and Bellarmine, T., "*Analysis of tone mapping operators on high dynamic range images,*" in *IEEE Proceedings*, Southeastcon, pp. 1-6, March, 2012.

[13] *E. Reinhards High Dynamic Range Data.*, (2014) [Online]. Available on: `http://www.cs.utah.edu/~reinhard/cdrom/hdr/`

[14] *G. Wards High Dynamic Range Data.*, (2014) [Online]. Available on: `http://www.anyhere.com/gward/pixformat/tiffluvimg.html`

[15] *P. Debevecs High Dynamic Range Data.*, (2014) [Online]. Available on: `http://www.debevec.org/Research/HDR/`

[16] *Zhou Wang TMQI Algorithm Data.*, (2014) [Online]. Available on: `https://ece.uwaterloo.ca/~z70wang/research/tmqi/`

[17] *Matlab HDR Toolbox & High Dynamic Range Data.* , (2014) [Online]. Available on: `http://in.mathworks.com/`

[18] *High Dynamic Range Data.*, (2014) [Online]. Available on: `http://resources.mpi-inf.mpg.de/hdr/calibration/pfs.html`

[19] L. Meylan and S. Ssstrunk, "*High Dynamic Range Image Rendering Using a Retinex-Based Adaptive Filter,*" in *IEEE Transactions on Image Processing*, Vol. 15, Nr. 9, pp. 2820-2830, 2006.

[20] Hee Kang, Suk Ho Lee, Ki Sun Song, and Moon Gi Kang, "*Bayer patterned high dynamic range image reconstruction using adaptive weighting function,*" in *EURASIP Journal on Advances in Signal Processing*, 2014:76, May. 2014.